SLAC–PUB–6359
October 1993
(T/E)

Semiexclusive Production in Electron-Positron Annihilation*

Thomas Hyer

Stanford Linear Accelerator Center

Stanford University, Stanford, California 94309

ABSTRACT

We present a thorough analysis of the direct semiexclusive production in quantum chromodynamics (QCD) of single, highly isolated mesons from electron-positron or two-photon initial states. Corrections of higher order and of subleading twist are considered, and potential divergences in the naive calculation are contained. Monte Carlo methods are used to relate the QCD calculations to experimentally measurable quantities. We find that the study of semiexclusive production is the most sensitive experimental probe of the structure of mesons in the valence ($q\bar{q}$) state at energies $\overline{s} \gtrsim 10$ GeV.

Submitted to *Physical Review D*

* Work supported by Department of Energy contract DE–AC03–76SF00515.

1. Introduction

1.1 Qualitative

To study Quantum Chromodynamics (QCD) in the real world is to study hadrons. The confinement of color, and the complicated structure of color-singlet hadronic states, presents the greatest obstacle to the study both of QCD itself and of other physics at hadron colliders, which will be masked by QCD effects. Similarly, the study of weak processes such as $b \to s\gamma$ is complicated by the dependence on meson wavefunctions of the observed hadronic rates. Thus it is essential to gain the greatest possible understanding of the structure of hadrons in preparation for future experiments.

The study of hadronic properties through exclusive processes [1] is by now an established industry. Grozin and Baier [2] and more recently Hyer [3] have proposed an alternative process, dubbed *semiexclusive* production, whose analysis holds promise of illuminating the structure of mesons with greater precision than is achievable with exclusive reactions.

Exclusive processes, in which the final state is completely specified, are inevitably suppressed by powers of Q^2 at high energies, where Q is the momentum scale apposite to the hard process under consideration [1]. The degree of this suppression in the amplitude can be shown to be $(\mu/Q)^{n_s}$, where $\mu \sim \Lambda_{\rm QCD}$ is a typical hadronic momentum scale and $n_s = n_{\rm partons} - n_{\rm hadrons}$ is the number of 'spectators' to the hard scattering, which must emerge collinear to the hadrons they constitute [4]. For example, the proton form factor falls like Q^{-4}, so that the associated cross sections are proportional to Q^{-10}.

In semiexclusive reactions, we specify the properties of one directly produced meson and demand a high degree of isolation (*e.g.*, isolation in a hemisphere in the center-of-momentum frame, or by a large rapidity gap) in order to eliminate inclusive backgrounds. Since we do not specify the content of the recoil system, we pay the minimum possible penalty in the cross section: there is only a single spectator quark. Thus semiexclusive meson production, which will be the focus of this paper [5], occurs with cross sections proportional to Q^{-4} (compared to total event cross sections of order Q^{-2}). For example, consider the current data sample of the CLEO detector at CESR, about 2 fb^{-1}. This represents about 10^7 events of all types. The semiexclusive production cross sections are about 2–3 fb for each meson, so several such events are expected even in the current data sample. On the other hand, the cross section for exclusive $\pi^+\pi^-$ production is on the order of 1 fb, and that for $p\bar{p}$ production is about 10^{-2} fb.

The less drastic suppression of semiexclusive cross sections with increasing energy allows us to study these processes at higher energies than the study of exclusive processes can reach, putting us in a region where the perturbation expansion is more reliable, and higher-twist terms more thoroughly suppressed.

Semiexclusive processes have a further advantage in the study of hadronic structure; the fraction z of the beam energy carried by the isolated meson can be measured, and the differential cross-section $\mathrm{d}\sigma/\mathrm{d}z$ reconstructed. The shape of this cross section depends on the distribution amplitude of the isolated meson; thus extraction of valence distribution amplitudes with high precision should become feasible. This is in contrast to the situation in purely exclusive scattering in which the angular distribution is trivial (as is the case for form factors) or is insensitive to the distribution amplitude [6,7] .

These advantages are partially, but not entirely, neutralized by the added complications due to the hadronization of the recoil system, which introduces nonperturbative physics into the computation of experimental results. Much of this work focuses on the extraction of viable results which take into account the behavior of the hadronizing system.

1.2 Quantitative

Our computational scheme is that of Lepage and Brodsky [1]. The amplitude for any process in which a 'hard' scale Q can be identified is written as a convolution of a hard-scattering subprocess amplitude, calculable in perturbative QCD (pQCD), with one or more process-independent nonperturbative light-cone hadron wavefunctions:

$$\mathcal{M} = \sum_i \int \mathrm{d}x\ \mathrm{d}^2k_\perp\ T_{Hi}(x, k_\perp; Q)\psi_i(x, k_\perp; Q), \tag{1.1}$$

where T_H is a pQCD amplitude for the hard scattering of free partons, ψ_i is the projection of the wavefunction onto the i^{th} Fock state, and Q is the 'separation scale' above which processes are deemed hard; processes with momentum transfer smaller than Q are absorbed into the wavefunction.

To leading twist, we may ignore the dependence of T_H on $k_\perp \sim \mu \ll Q$. Then, defining [8]

$$\phi(x; Q) \equiv \int^Q \mathrm{d}^2k_\perp\ \psi(x, k_\perp; Q), \tag{1.2}$$

we obtain the simpler form (valid up to terms of $O(\mu^2/Q^2)$ where $\mu \lesssim 1$ GeV is a typical hadronic momentum scale)

$$\mathcal{M} = \int \mathrm{d}x\ T_H(x; Q)\phi(x; Q). \tag{1.3}$$

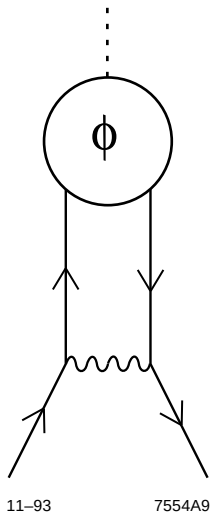

Figure 1. Feynman diagrams contributing to the semiexclusive process $e^+e^- \to HX$. Here we show only the hadronic event topology; a sum over all possible attachments of the incoming γ^* is assumed. All external particles are outgoing; arrows indicate fermion flow.

Another crucial simplification results from the neglect of all terms of higher twist: the amplitude thus calculated depends only on the projection of the wavefunction onto the Fock state of smallest particle number and with no orbital angular momentum, the 'valence' Fock state [1]. Thus the tremendous complexity of the hadronic structure is reduced to the single valence distribution amplitude ϕ. Gupta [9] has shown that the factorization theorems from exclusive processes are also valid in the semiexclusive case, so that the distribution amplitudes extracted from the study of semiexclusive processes are indeed universal.

Figure 1 shows the Feynman diagrams contributing at tree level to the simplest semiexclusive process, $e^+e^- \to K^-X$ (of course, any light meson may be produced by the same mechanism). In this work, we will systematically explore the properties of the resulting system, obtaining a set of reliable predictions of experimentally measurable quantities.

This paper is organized as follows: Section 2 computes the tree-level amplitudes at leading twist for the processes of interest and comments on their structure.

Section 3 is devoted to next-to-leading twist corrections to these results, arising from the inclusion of quark and meson mass terms, intrinsic transverse momenta, and higher Fock states. Section 4 explores the effects of Sudakov suppression and the running of the QCD coupling α_s. Section 5 describes the effects of other higher-order pQCD processes on our results. Section 6 explores the collinear divergence of the naive tree-level amplitude which arises when one quark is created nearly parallel to the produced meson; a more accurate, convergent form is used for this region, and the effect on measurements away from the collinear region is explored. Section 7 uses standard Monte Carlo methods to study the relation between the isolation of the directly produced meson in the partonic system and the experimentally measured isolation from hadrons produced in fragmentation. Finally, Section 8 presents our results, extracts experimentally accessible quantities, and discusses the prospects for constraining hadronic distribution amplitudes.

2. Tree-level amplitudes

In this chapter, we calculate the tree-level amplitudes for the semiexclusive process $e^+e^- \to HX$, where H is some meson. The amplitudes take their simplest form in the center-of-momentum frame if we define [3]

the hadron momentum fraction

$$z \equiv \frac{E_H + |\vec{p}_H|}{\bar{s}};$$

the antiquark and quark (respectively) back-momenta (light-cone momenta in the frame antiparallel to $\vec{p}_H$)

$$y_{i \quad \bar{s}} \equiv E_i - \frac{\vec{l}_i \cdot \vec{p}_H}{|\vec{p}_H|},$$

with $y_1 + y_2 = 1 - m_H^2/zQ^2$;

the beam scattering angles θ and ϕ, where θ is the e^--to-H polar angle, and ϕ is the angle between the H-q-$\bar{q}$ plane and the plane containing the beam and H [10]; and

$s \equiv \sin(\theta/2)$ and $c \equiv \cos(\theta/2)$.

In these terms, the unpolarized differential cross section is

$$\mathrm{d}\sigma = \frac{1}{1024\pi^4}\, z\bar{z}\mathrm{d}z\ \mathrm{d}y_1\ \mathrm{d}\Omega\ \frac{1}{2} \sum_{\text{spins}} |\mathcal{M}|^2, \tag{2.1}$$

where we have introduced the notation $\bar{z} \equiv 1 - z$; recall that $\mathcal{M}$, for a process with three final-state particles, has dimensions of mass^{-1}.

For leading-twist calculations, we use the helicity formalism of Ref. [11]; the spinors and polarization vectors are tabulated in Appendix A. We do not need to compute the interference effects between different quark helicity amplitudes, even if the resulting hadron helicities are identical, because our neglect of resonance effects in the recoil system is tantamount to treating the recoil quarks as observable particles. Thus pseudoscalar states $|+-\rangle - |-+\rangle$ and longitudinally polarized vector states $|+-\rangle + |-+\rangle$ will yield identical hard-scattering amplitudes.

This assumption means that our results will be valid only in the region in which duality holds; we expect that it will be very accurate when the invariant mass $\bar{z}Q^2$ of the hadronizing recoil system is larger than about $(2\ \mathrm{GeV})^2$ [12]. This will provide an upper limit on the values of z at which our computed cross sections are reliable; however, at $Q \sim 10$ GeV the restriction is almost unnoticeable due to the factor of $\bar{z}$ in Eq. (2.1), which ensures that the differential cross section $\mathrm{d}\sigma/\mathrm{d}z$ vanishes as $z \to 1$.

2.1 Distribution amplitudes

To leading twist, the hadron wavefunction enters only through the valence-state distribution amplitude of Eq. (1.2). In eqs. (1.2) and (1.3), we will let x denote the light-cone momentum fraction carried by the heavier parton, be it quark or antiquark. Thus we expect $\langle x \rangle \geq 0.5$.

While the asymptotic behavior of the distribution as $Q^2 \to \infty$ is simple and well understood, the approach to asymptopia is very slow [1]. One interesting approach to extraction of distribution amplitudes at moderate Q^2 is the sum-rule approach [13-16]. This method relates moments of the distribution, of the form

$$\int_0^1 (x - \bar{x})^n \phi(x) \mathrm{d}x,$$

to the observed spectrum of hadron masses. It has so far yielded predictions in good agreement with experiment ; one of our aims is to provide a more precise test of its accuracy.

Since the distribution amplitude must vanish like $x\bar{x}$ at each endpoint, it is customary to expand it as a series of Gegenbauer polynomials [18], which are orthogonal under the measure with weight $x\bar{x}$:

$$\phi(x) = \frac{f_h}{2} x\bar{x} \sum_{i=0}^{\infty} a_i P_i(x), \quad \text{where} \int_0^1 x\bar{x} P_i(x) P_j(x) \mathrm{d}x = \delta_{ij}, \tag{2.2}$$

and f_h is the hadron decay constant, which can be measured experimentally in semileptonic decay.

A major advantage of this expansion is that the Gegenbauer polynomials are the eigenfunctions of the one-loop evolution equation for the meson valence

distribution amplitude [1]. Thus the running of the coefficients a_i is simple and easily calculable. We will take advantage of this fact in our analysis of semiexclusive production in Z decays (Section 2.7). Our normalization ensures that a_0, which does not run with increasing Q^2 for scalar or longitudinally polarized mesons [1], is equal to 1.

The first few Gegenbauer polynomials are [19]

$$\begin{aligned}
P_0 &= \overline{6} \\
P_1 &= \overline{30}(x-\bar{x}) \\
P_2 &= 2\ \overline{21}(1-5x\bar{x}) \\
P_3 &= 6\ \overline{5}(x-\bar{x})(1-7x\bar{x}) \\
P_4 &= \overline{330}(42x^2\bar{x}^2-14x\bar{x}+1) \\
P_5 &= \overline{546}(x-\bar{x})(66x^2\bar{x}^2-18x\bar{x}+1)\ldots
\end{aligned} \tag{2.3}$$

To proceed from the moments derived from QCD sum rules to definite models of the distribution amplitude, we fit the required moments with a sum over the first few Gegenbauer polynomials. In general, it is far simpler to test the resulting model than to extract the moments from experiment; however, the resulting confrontation with theory is somewhat oblique. We will discuss the problem of addressing the sum-rule predictions more directly in Section 8.5.

We will find it useful to define the integrals [3]

$$
\begin{aligned}
A(z) &\equiv \int_0^1 \frac{\phi(x)}{\bar{x}(1-zx)}\mathrm{d}x, \quad \bar{A}(z) \equiv \int_0^1 \frac{\phi(x)}{x(1-z\bar{x})}\mathrm{d}x; \\
B &\equiv A(0) = \int \frac{\phi(x)}{\bar{x}}\mathrm{d}x, \quad \bar{B} \equiv \bar{A}(0); \\
C(z) &\equiv \int_0^1 \frac{\phi(x)}{x\bar{x}(1-zx)}\mathrm{d}x, \quad \bar{C}(z) \equiv \int_0^1 \frac{\phi(x)}{x\bar{x}(1-z\bar{x})}\mathrm{d}x, \\
\text{and} \quad D &\equiv C(0) = \bar{C}(0) = \int_0^1 \frac{\phi(x)}{x\bar{x}},
\end{aligned}
\tag{2.4}
$$

which control the behavior of the cross section. These quantities are related by

$$
C(z) = zA(z) + D, \quad \bar{C}(z) = z\bar{A}(z) + D, \qquad \text{and} \quad D = B + \bar{B}.
$$

Note that A and C are logarithmically divergent as $z \to 1$; however, we find that their contributions to cross sections are always suppressed by one or more powers of $1 - z$, so that we obtain consistently finite results. The Dirac form factors of mesons are determined solely by B and $\bar{B}$: *e.g.*, $F^1_{K^-} \propto |q_s B_K^2 - q_u \bar{B}_K^2|$.

The foremost goal, when measuring the semiexclusive cross section, is the precise extraction of the functions $A(z)$ and $\bar{A}(z)$, from which the distribution amplitude $\phi(x)$ may be reconstructed. In terms of the Gegenbauer coefficients of Eq. (2.2), these integrals can be written

$$A(z) = -\frac{f_H}{\overline{2}} \sum_{i=0}^{\infty} \text{FINITE}\ \frac{a_i P_i(z^{-1}) \ln(1-z)}{z^2}\ ;$$

$$\bar{A}(z) = -\frac{f_H}{\overline{2}} \sum_{i=0}^{\infty} \text{FINITE}\ \frac{(-1)^i a_i P_i(z^{-1}) \ln(1-z)}{z^2}\ ;$$

$$B = \frac{f_H}{\overline{2}} \sum_{i=0}^{\infty} a_i \quad \overline{\frac{2i+3}{(i+1)(i+2)}};$$

$$\bar{B} = \frac{f_H}{\overline{2}} \sum_{i=0}^{\infty} (-1)^i a_i \quad \overline{\frac{2i+3}{(i+1)(i+2)}};$$

$$C(z) = -\frac{f_H}{\overline{2}} \sum_{i=0}^{\infty} \text{FINITE}\ \frac{a_i P_i(z^{-1}) \ln(1-z)}{z}\ ;$$

$$\bar{C}(z) = -\frac{f_H}{\overline{2}} \sum_{i=0}^{\infty} \text{FINITE}\ \frac{(-1)^i a_i P_i(z^{-1}) \ln(1-z)}{z}\ ; \text{and}$$

$$D = \frac{f_H}{\overline{2}} \sum_{i=0}^{\infty} \left(1 + (-1)^i\right) a_i \quad \overline{\frac{2i+3}{(i+1)(i+2)}}.$$

Here we define FINITE$[f(x)]$ to be the finite part of the Laurent expansion of f in x (or, equivalently, the residue after $x \to 0$ divergences have been removed by minimal subtraction); for instance,

$$\begin{aligned} \text{FINITE}\ \frac{-\ln(1-x)}{x^3} &= \text{FINITE}\ x^{-2} + \frac{x^{-1}}{2} + \frac{1}{3} + \frac{x}{4} + \cdots = \frac{1}{3} + \frac{x}{4} + \cdots \\ &= \frac{-\ln(1-x) - x - x^2/2}{x^3}. \end{aligned}$$

2.2 Modeling the distribution amplitude

To obtain concrete predictions for production cross sections, we must have a specific model of the distribution amplitude. The simplest 'model' is simply the known asymptotic form [1]:

$$\phi(x) = f_H \quad \overline{3}\ x\bar{x}. \tag{2.5}$$

Table 1

Distribution	Coefficients				Integrals	
	a_0	a_1	a_2	a_3	B	$\bar{B}$
Asymptotic	1.0	0	0	0	$0.87 f_h$	
ZZC K	1.0	0.24	0.64	0.13	$1.43 f_K$	$0.99 f_K$
ZZC π	1.0	0	1.07	0	$1.44 f_\pi$	
ZZC ρ_L	1.0	0	0.27	0	$1.01 f_\rho$	
ZZC ρ_T	1.0	0	-0.27	0	$0.72 f_\rho$	
ZZC K_L^*	1.0	0	0.11	0	$0.93 f_{K^*}$	
ZZC ϕ	1.0	0	-0.05	0	$0.84 f_\phi$	
Toy K	1.0	0.45	0	0	$1.16 f_K$	$0.58 f_K$
'stealth' K	1.0	0.34	0.64	0	$1.43 f_K$	$0.99 f_K$

However, there is good reason to believe that the distribution amplitudes at moderate Q^2 are very different: predictions of exclusive cross sections based on this distribution, for example, systematically predict values far below the experimental results [13].

The distribution amplitudes predicted from QCD sum rules are in substantially better agreement with present experimental results [14–17]. Table 1 presents the coefficients of the Gegenbauer polynomials in the models we use. We also present the coefficients for two toy models, which we will use for purposes of comparison to test the power of the analysis. The first of these models is the simple toy model [3]

$$\phi_K(x) = 2 \quad \overline{3} f_K x^2 \bar{x},$$

which we will use for strange mesons; the second is a 'stealth' model, with the coefficients a_1 and a_2 chosen such that the integrals B_K and $\bar{B}_K$ match those from

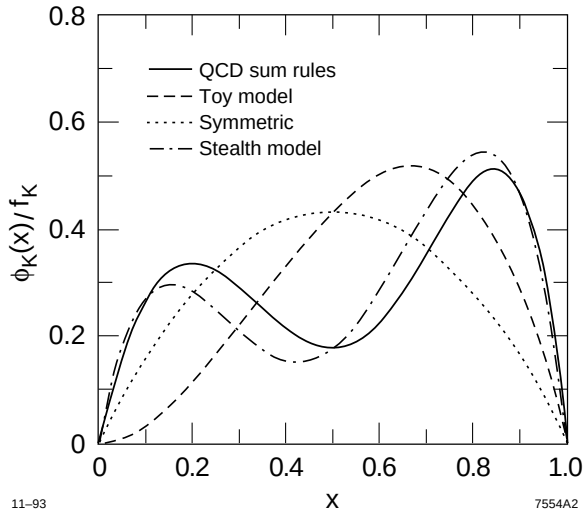

Figure 2. Models of the distribution amplitude ϕ_K. The curve marked 'QCD sum rules' is the model of Ref. [15]; the symmetric curve shows the asymptotic large-Q limit. The toy and 'stealth' models are described in the text.

the ZZC sum-rule model. The stealth model necessarily bears a strong resemblance to the sum-rule model, as shown in Fig. 2. The resemblance of the transforms $A(z)$ and $\bar{A}(z)$ is even more extreme; in fact, $A(z)$ and $\bar{A}(z)$ differ by no more than 6% over the range $z < 0.95$, and these differences are strongly anticorrelated, as shown in Fig. 3. Thus the stealth wavefunction serves to illustrate the range of variation in the distribution which can be concealed in semiexclusive production. Of course, the ZZC and stealth distributions yield precisely the same Dirac form factor as well.

Figure 4 shows the model wavefunctions obtained by a fit to the sum-rule moment predictions for the π and ρ mesons [14,15]. The symmetry of these wavefunctions under $x \to \bar{x}$ implies $A(z) = \bar{A}(z)$. A striking prediction of the sum rules is that ϕ_π is strongly peaked near the endpoints, giving it the bimodal structure shown; in contrast, ϕ_{ρ_T} is strongly peaked at $x = 1/2$ and drops off sharply near the endpoints. Thus it is predicted that the transform $A_\pi(z)$ will be much greater than $A_\rho(z)$, and the cross section correspondingly larger.

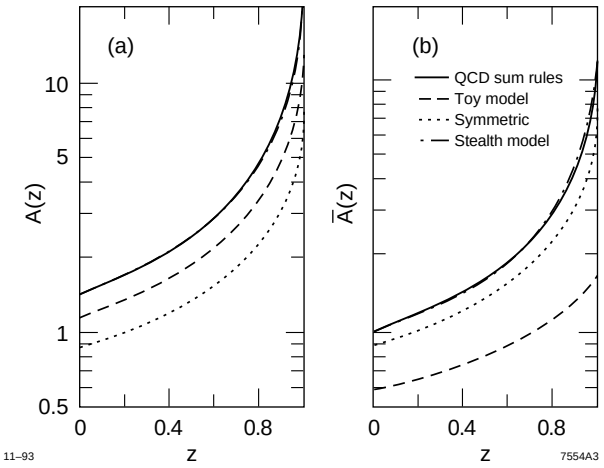

Figure 3. The transforms $A_K(z)$ and $\bar{A}_K(z)$ corresponding to the distribution amplitudes shown in Fig. 2. Note the extremely close resemblance between the 'stealth' model and the sum-rule model prediction.

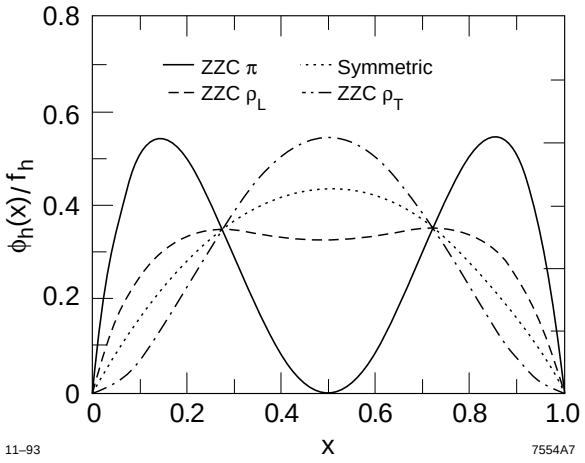

Figure 4. Sum-rule distribution amplitudes for the π and ρ mesons [14,16].

2.3 Evolution of the distribution amplitude

The sum-rule models are obtained at a momentum transfer $Q_0^2 \simeq 1.5$ GeV^2; since the processes in which we are interested probe the distribution amplitude at somewhat larger Q^2, we must take the evolution of the distribution into account. Since the Gegenbauer polynomials are eigenfunctions of the evolution equation, this is easily accomplished by the substitution [1]

$$a_n(Q^2) = a_n(Q_0^2)\ \frac{\ln(Q^2/\Lambda^2)}{\ln(Q_0^2/\Lambda^2)}\ ^{-\gamma_n}, \quad \text{where } \gamma_n \equiv \frac{C_F}{\beta}\Big(1{+}4\sum_{k=2}^{n+1}\frac{1}{k}{-}\frac{2\delta_{\lambda\bar{\lambda}'}}{(n+1)(n+2)}\Big),$$

$C_F = 4/3$ is the color factor, $\beta = 11 - 2/3n_f$ is the one-loop QCD beta function, λ and λ' are the quark and antiquark helicities within the pion, and $\bar{\lambda}' \equiv -\lambda'$. For pseudoscalar or longitudinally polarized mesons, $\delta_{\lambda\bar{\lambda}'} = 1$, and the first few anomalous dimensions γ_n are

$$\gamma_0 = 0, \qquad \gamma_1 = \frac{8C_F}{3\beta}, \qquad \gamma_2 = \frac{25C_F}{6\beta}, \qquad \text{and} \quad \gamma_3 = \frac{157C_F}{30\beta};$$

for transversely polarized vector mesons, $\delta_{\lambda\bar{\lambda}'} = 0$, and

$$\gamma_0 = \frac{C_F}{\beta}, \qquad \gamma_1 = \frac{3C_F}{\beta}, \qquad \gamma_2 = \frac{13C_F}{3\beta}, \qquad \text{and} \quad \gamma_3 = \frac{16C_F}{3\beta}.$$

It is noteworthy that the quark mass terms do not enter into the evolution potential [1,20]. Thus heavy-quark mesons evolve in the same way as light mesons. We expect that at low momentum transfer the heavy quark will carry a large momentum fraction, so that $1 - \langle x\rangle \ll 1$; thus it is worth while to consider the evolution of $\langle x\rangle$ with Q^2. We find that in terms of the parameter

$$\xi \equiv \ln\ln\frac{Q^2}{\Lambda^2},$$

the heavy-quark momentum fraction obeys the evolution equation

$$\frac{\mathrm{d}}{\mathrm{d}\xi}\langle x\rangle = -\Big(1 + \frac{\delta_{\lambda\bar{\lambda}'}}{3}\Big)\frac{C_F}{\beta} + O(1 - \langle x\rangle),$$

independent of the shape of the distribution amplitude. Thus we derive the approximate relation for heavy-light pseudoscalar mesons

$$\big\langle x; Q^2\big\rangle \simeq \big\langle x; Q_0^2\big\rangle - \frac{4C_F}{3\beta}\Big(\ln\ln\frac{Q^2}{\Lambda^2} - \ln\ln\frac{Q_0^2}{\Lambda^2}\Big).$$

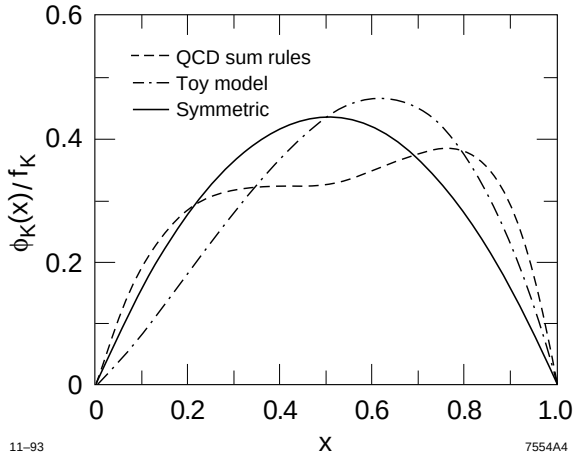

Figure 5. The distribution amplitudes of Fig. 2, evolved to $Q = m_Z$.

For $Q_0^2 = 1.5$ GeV^2 and $\langle x; Q_0^2 \rangle = 0.95$, this implies $\langle x; Q^2 = (10 \text{ GeV})^2 \rangle \sim 0.79$ and $\langle x; Q^2 = m_Z^2 \rangle \sim 0.70$. Clearly the $O(1-\langle x \rangle)$ corrections begin to be important before this stage; nonetheless, we see that the evolution of the distribution amplitude will quickly smooth any sharp peaks. Since a substantial cross section for semiexclusive production at very high energies, *e.g.* in Z decays, depends on a strongly peaked distribution amplitude [3], consideration of the evolution of the distribution amplitude greatly decreases both the expected cross sections and the efficacy with which we will be able to discriminate among models; see Fig. 5. We will return to this point in Sections 8.3 and 8.4.

2.4 Mesons with flavor

In the production of mesons with a nonzero flavor quantum number (including isospin), only the four Feynman diagrams of Fig. 1 contribute. We will specialize to the case $H = K^-$ or $H = K^{*-}$, for the sake of definiteness; of course, our results are equally valid for all light flavored mesons. In addition, we will omit an overall factor of $e^2 g_s^2/Q^2 = 16\pi^2 \alpha \alpha_s/s$, which is understood to be included in all the amplitudes we will present.

For pseudoscalar mesons or longitudinally polarized vector mesons (*i.e.*, for anti-aligned quark spins) the hard-scattering amplitude is given in [3]:

$$T_H^{(+)} = C_F \Bigg\{ \frac{y_2\bar{x}q_u - y_1 x q_s}{zx\bar{x}\ \overline{y_1 y_2}} \Bigg[\Big(s e^{-i\phi} - \frac{\overline{\bar{z}y_2}}{y_1} c \Big) \Big(c - \frac{\overline{\bar{z}y_1}}{y_2} s e^{-i\phi} \Big) \Bigg] + \frac{1}{x} \frac{\overline{y_2}}{y_1} s e^{-i\phi} q_u \Big(c - \frac{\overline{\bar{z}y_2}}{y_1} \frac{s e^{-i\phi}}{1 - z\bar{x}} \Big) - \frac{1}{\bar{x}} \frac{\overline{y_1}}{y_2} c q_s \Big(s e^{-i\phi} - \frac{\overline{\bar{z}y_1}}{y_2} \frac{c}{1 - zx} \Big) \Bigg\}, \tag{2.6}$$

with the color factor $C_F = 4/3$. The superscript $(+)$ refers to the case in which the incoming electron and outgoing s quark share the same helicity; it is a simple matter to show that the opposite-helicity amplitude can be obtained by the substitution $c \leftrightarrow s$ (see Appendix A).

The corresponding amplitude for transversely polarized vector meson production is

$$T_H^{(+)} = c^2 \ \overline{\bar{z}} \Bigg[\frac{q_s}{\bar{x}(1 - zx)y_2} - \frac{q_u}{x(1 - z\bar{x})y_1} \Bigg]. \tag{2.7}$$

As noted in Ref. [3], these amplitudes do not vanish even in the limits $q_u \to q_s$ and $x \to \bar{x}$, unless we also impose $y_1 \to y_2$. The hard virtual photon probes the structure of the meson at the parton level.

The factor $\overline{\bar{z}}$ in Eq. (2.7) is also noteworthy; it leads to the vanishing of the amplitude in the exclusive limit, as required by hadron helicity conservation [21]. It must be noted that the light-cone wavefunctions of vector mesons depend on the polarization; thus the total unpolarized cross-section for vector meson production will sum contributions from two distinct distribution amplitudes. However, the simple $1 + \cos^2\theta$ angular distribution of the cross section for production in transverse polarization states should aid in disentangling the two

processes. Also, the decays of vector mesons are to some extent self-analyzing; the polarization of, *e.g.*, a ρ meson can be estimated from the angular distribution of its decay products. Thus at given z, the observed distribution at leading twist of semiexclusive events, integrated over $\mathrm{d}\phi$, should be an incoherent sum of three simple distributions (longitudinal with shape $\sin^2\theta$, and longitudinal or transverse with shape $1+\cos^2\theta$). Unfortunately, the cross section is dominated by the term proportional to $(1+\cos^2\theta)$, which mixes both transverse and longitudinal contributions with further contamination from backgrounds (which will have the $1+\cos^2\theta$ distribution common to inclusive processes). We will discuss the potential to extract the other components of the cross section; however, extremely large event samples seem necessary for such extraction.

2.5 Mesons without flavor

Some mesons, such as the η or π^0, have no nonzero flavor quantum numbers (excepting isospin). Thus they might be formed by diagrams like that of Fig. 6, recoiling against a gg system. Note that only pseudoscalar mesons can receive such a contribution at leading twist, as the quark and antiquark spins are anti-aligned.

For definiteness, we will consider $h=\eta$. In computing the amplitude for production of ηgg, we must sum over quark helicities and flavors (since in this case the helicities are no longer observable). We choose to absorb this factor in the hard-scattering amplitude; that is, we present the amplitude

$$\frac{1}{\overline{2}}\; T_H(e^+e^-\to q_+\bar{q}_-gg) - T_H(e^+e^-\to q_-\bar{q}_+gg)\;\;,$$

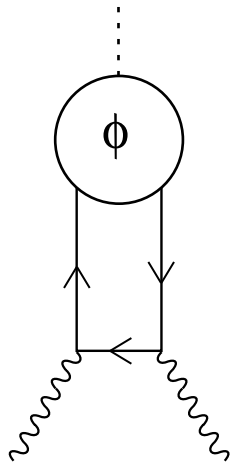

Figure 6. Additional Feynman diagrams which must be considered in the case of flavorless pseudoscalar mesons. As in Fig. 1, a sum over attachments of the incoming γ^* is implicit.

but call it T_H since we will obtain the full amplitude by convolving it with the distribution amplitude, as always. The result is

$$T_H(e^-_+e^+_- \to \eta g_\uparrow g_\uparrow) = C_F q_i s^2 \quad \overline{\frac{2\bar{z}}{y_{\min}y_{\max}}}\left(\frac{1}{x(1-z\bar{x})} - \frac{1}{\bar{x}(1-zx)}\right); \tag{2.8}$$

$$T_H(e^-_+e^+_- \to \eta g_\uparrow g_\downarrow) = \frac{C_F q_i}{zx\bar{x}} \quad \overline{\frac{\bar{z}}{2y_\uparrow y_\downarrow}}\,(c^2 y_\downarrow - s^2 e^{2i\phi} y_\uparrow)\left(\frac{1}{1-zx} - \frac{1}{1-z\bar{x}}\right); \tag{2.9}$$

$$T_H(e^-_+e^+_- \to \eta g_\downarrow g_\downarrow) = C_F q_i c^2 \quad \overline{\frac{2\bar{z}}{y_{\min}y_{\max}}}\left(-\frac{1}{x(1-z\bar{x})} + \frac{1}{\bar{x}(1-zx)}\right). \tag{2.10}$$

In this case, the color factor is $C_F = \overline{2/3}$, not $4/3$. In Eq. (2.9), we have used the notation $y_{\uparrow,\downarrow}$ instead of $y_{1,2}$ to refer to the two gluon momenta, since the labels 1 and 2 are arbitrary; in Eqs. (2.8) and (2.10), we define $y_{\min} = \min\{y_i\}$ and $y_{\max} = \max\{y_i\}$.

The amplitudes for negative-helicity electrons (positive-helicity positrons) are obtained, as always, by the substitution $s \leftrightarrow c$ (Appendix A). However, in either case, the amplitudes of Eqs. (2.8)–(2.10) are antisymmetric under $x \leftrightarrow \bar{x}$. The wavefunction must be symmetric; thus the full amplitude, obtained by convolving

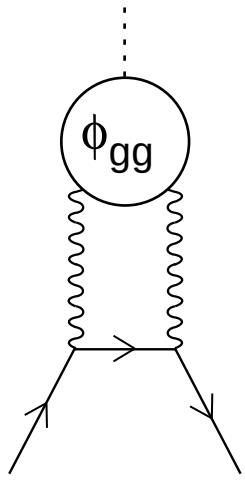

Figure 7. Feynman diagrams contributing to production of a meson in a gg Fock state. Again, a sum over attachments of the γ^* is implicit.

ϕ with T_H, vanishes. We need not treat such mesons any differently than we would flavored states.

2.6 Mesons with gg Fock states

Scalar mesons, with spin-parity 0^+, have no $q\bar{q}$ valence Fock state but can mix with a gg state. The lightest and best measured such meson is the $f_0(975)$, which we now consider.

Production in the gg Fock state recoiling against a $q_i\bar{q}_i$ system, shown in Fig. 7, proceeds with the hard-scattering amplitude

$$T_H = -C_F \frac{q_i}{2zx\bar{x}y_1y_2} \quad \bar{\bar{z}}y_2(1-zx^2)c^2+2 \quad \overline{y_1y_2}(zx\bar{x}+\bar{z})sce^{i\phi}+ \quad \bar{\bar{z}}y_1(1-z\bar{x}^2)s^2e^{2i\phi} \ ; \tag{2.11}$$

again, the color factor $C_F = \quad \overline{2/3}$.

In Eq. (2.11) the quark spins are considered observables, and the quark and antiquark are distinguishable, in contrast to Eq. (2.9) in which we sum over spin states in the amplitude, leading to destructive interference in the large-z limit and

to antisymmetry under $x \leftrightarrow \bar{x}$. This should emphasize the importance of studying semiexclusive processes only in the domain in which the assumption of duality is accurate; in the exclusive limit $z \to 1$, the processes corresponding to Eqs. (2.9) and (2.11) become identical, and both amplitudes vanish.

The result of Eq. (2.11) shows that the amplitude for scalar meson production in a gg Fock state depends on the distribution amplitude through the quantity

$$f_{h\to gg} \equiv 2 \quad \overline{3} \quad \int_0^1 \phi_{h\to gg}(x)\mathrm{d}x, \tag{2.12}$$

where the constant factor is analogous to that of Eq. (2.2), and through the integrals B_{gg}, $\bar{B}_{gg}$, and D_{gg}, as defined in Eq. (2.4), where the subscript gg reminds us that the distribution amplitude in question is $\phi_{h\to gg}$. However, the distribution amplitude must be symmetric under $x \leftrightarrow \bar{x}$, so we have $B_{gg} = \bar{B}_{gg} = D_{gg}/2$.

The lack of valence $q\bar{q}$ Fock states of 0^+ mesons is a boon to our analysis; any observation of $f_0(975)$ production at leading twist is an unambiguous signal of formation in the gg Fock state. The $f_0(975)$ decays primarily to $\pi\pi$, which should provide a clear experimental signal if it can be distinguished from $\rho(770) \to \pi\pi$.

We can also compute the amplitude for creation of transversely polarized 2^+ mesons in the gg Fock state by requiring that the gluon spins be aligned. The amplitude for this process is

$$T_H{}^{(++)} = -C_F q_i \frac{\bar{\bar{z}}}{z^2 x\bar{x}} \frac{1}{y_1 y_2} (c \quad \overline{y_2} + s e^{i\phi} \quad \overline{\bar{z}y_1})(c \quad \overline{\bar{z}y_1} - s e^{i\phi} \quad \overline{y_2}) \tag{2.13}$$

when the gluons have the same helicity as the electron and the outgoing antiquark; the other amplitudes are obtained by $y_1 \leftrightarrow y_2$ and $s \leftrightarrow c$. The lightest such

meson is the $f_2(1270)$; again, its signature is decay to $\pi\pi$. The most important backgrounds in this case come from the $f_0(1400)$ and $\rho(1450)$, both of which can also decay to two pions. Also, the suppression of higher-twist terms is less severe at larger mass, so that contamination from $q\bar{q}$ states with $L = S = 1$ must be considered. We will touch upon this point again in Section 3.3.

Semiexclusive production cross sections for 2^{++} mesons, like those for 1^{--} mesons, sum contributions from the transverse and longitudinal polarization states. Thus the quantities $f_{h\to g_\uparrow g_\downarrow}$, $D_{gg/L}$, and $D_{gg/T}$, where the subscripts L and T denote transverse and longitudinal polarization states, will contribute to the measured cross section for $f_2(1270)$ production. We will display our predictions in Section 8.1.

2.7 Z^0 DECAYS

The channel $e^+e^- \to Z^0 \to HX$ can also contribute to semiexclusive production. Although the suppression by μ^2/Q^2 is far more severe at the Z peak than at the energies we have so far considered, we can still obtain detectable cross-sections.

Bjorken *et al.* [22,23] have pointed out that the requirement of a rapidity gap is a natural and effective way to identify processes involving production of color singlets. That is, we may require that the candidate directly-produced meson be isolated in rapidity (or pseudorapidity) with respect to its own axis by some gap ΔY. Indeed, the condition of isolation in a hemisphere can be thought of as a special case of the rapidity gap, where $\Delta Y = \ln(2zE/m_H)$ is a function of z.

For light mesons, *e.g.* $H = K$, isolation in a hemisphere is equivalent to $\Delta Y = 6 + \ln z$. This is unnecessarily drastic; values of $\Delta Y \simeq 4$ should be more than adequate to screen out backgrounds from the hadronization process [24].

Following Ref. [23], we write the weak charge of a fermion as

$$\mathbf{Q}_f \equiv \begin{pmatrix} Q_{f_L} \\ Q_{f_R} \end{pmatrix}, \tag{2.14}$$

containing both the right- and left-handed couplings to the Z. Then the amplitudes for semiexclusive production in Z decays can be obtained from those derived in the last two sections by the simple substitution $q_f \to \mathbf{Q}_f$, with the understanding that the dot product $\mathbf{Q}_{f_1} \cdot \mathbf{Q}_{f_2}$ is to replace the sum over spins $q_{f_1} q_{f_2}$ in the unpolarized cross-section.

We will later see that while the cross sections are much smaller at this energy, the experimental separation of interesting higher-twist physics is somewhat easier. Thus we can hope to observe semiexclusive Z^0 decays.

2.8 Crossing

It should be noted that semiexclusive production $e^+e^- \to HX$ is the crossed process corresponding to deep inelastic scattering (DIS) $e^-H \to e^-X$. Thus we expect the cross-sections calculated here to bear some relation to the structure functions of DIS.

Indeed, carrying out the crossing operation and evaluating the variables q^2 and x governing DIS, we find $q^2 = -Q^2$, $x = z^{-1}$. Thus semiexclusive production can be said to measure the continuation of the structure function to the region $x > 1$. Indeed, the quantity $[A(z)]^2$ of Eq. (2.4) for $z > 1$ shows some properties

of a structure function, with a leading-twist pole contribution at $x = z^{-1}$; the resemblance would be more pronounced had we not implemented the simplification of Eq. (1.2).

As we shall see in Section 6, this pole corresponds to the collinear singularity at $y_i = 0$ in semiexclusive production. Part of our task will be to separate the interesting but higher-twist central region where y_i is not small from contamination due to the collinear pole.

3. Higher-twist corrections

So far, we have been concerned with the leading-twist behavior of semiexclusive amplitudes. In obtaining our results so far, we have made several simplifying assumptions:

- We have neglected all quark masses, which give rise to corrections of order m^2/Q^2 to the helicity amplitudes we have calculated and introduce helicity-flip amplitudes at order m/Q [21].
- We have neglected the mass of the meson H as well as that of the hadronizing quarks in defining our kinematic variables; a more careful definition will change our results by terms on the order of m_H^2/Q^2.
- We have assumed that the quark constituents are perfectly collinear with the hadron comprising them; if we relax this assumption to allow quark transverse momenta $k_\perp$, we will obtain a correction of order $k_\perp^2/Q^2$ [25]. In addition, we have entirely neglected the effects of Sudakov suppression [26] on the amplitude.
- Finally, we have considered only the valence Fock state of the meson, and ignored the possibility of mixing with qqg states. The corrections resulting

from a correct treatment of such states, while still suppressed by μ^2/Q^2, have the potential to be numerically large because of the contribution they receive from the endpoints of the distribution amplitude, when one of the constituent partons is very soft.

Let us deal with these corrections, one at a time.

3.1 Quark and meson mass effects

Terms of order m/Q in the amplitude involve helicity flips; thus they will contribute only at order m^2/Q^2 to the cross section, as will interference terms between leading-twist amplitudes and $O(m^2/Q^2)$ corrections. We can only hope to distinguish contributions of subleading twist if they show some signature distinguishing them from the leading-twist cross section, which the interference terms will not have. Thus we do not consider such terms, but instead choose to restrict our discussion to the computation of the leading helicity-flip amplitudes.

We account for quark mass terms to first order in m/Q in internal lines by computing all single Higgs insertions on the internal quark line. The effect of mass insertions on external lines is to alter the quark spinor by the substitution (see Appendix A)

$$u_\pm(p) \to u_\pm(p) + \frac{m}{E+|\vec{p}|} u_{(\pm\to\mp)}(p) + O(m^2); \tag{3.1}$$

$u_{(\pm\to\mp)}$ considered as a two-component spinor is numerically identical to $u_\pm$, but corresponds to opposite helicity (*i.e.*, $u_{(\pm\to\mp)} = \gamma^0 u_\pm$, while $v_{(\pm\to\mp)} = -\gamma^0 v_\pm$).

Since we are interested in obtaining quantities with experimental signatures distinct from those of leading-twist semiexclusive production, we must consider the production of transversely polarized vector mesons with an angular distribution other than the $(1+\cos^2\theta)$ distribution obtained from Eq. (2.7).

As an example, we consider the amplitude for $e^+e^- \to D^*_\uparrow \bar{c}_+ u_-$. Naively calculating with the substitution of Eq. (3.1) yields a divergent expression from the region $x \to 0$, in which the quantity m/xzQ becomes large. In this limit, of course, the first-order expansion in m is invalid. We choose to contain the divergence by keeping terms of order m^2 in the gluon denominator $(xp + l_1)^2$, which yields uniformly finite expressions.

We are interested in the part of the above amplitude which is proportional to $sce^{i\phi}$. This is (omitting the usual factor of $e^2 g_s^2/Q^2$)

$$-\frac{m_c}{Q}\frac{\overline{\bar{z}}}{zx}\left[\frac{2}{z\bar{x}}\frac{y_1}{y_2}q_c + \frac{z + 2\bar{z}y_2}{xy_1 + \bar{z}y_2 m_c^2/z^2 x}q_u\right]. \tag{3.2}$$

The expression in brackets is not numerically large, especially when one considers that the wavefunction is likely concentrated at fairly large x. In fact, it is generally smaller than the amplitude of Eq. (2.7), even before the m/Q suppression is taken into account. Thus the higher-twist contribution to the cross section from quark mass terms will be not more than $m_{\mathbf{q}}^2/Q^2$: 3% for D mesons at the Υ_{4s}, and less than 0.5% for B mesons at the Z^0 peak. Since such terms must be disentangled from both the $(1 + \cos^2\theta)$ distribution of most semiexclusive events and the $\sin^2\theta$ component of the distribution of longitudinally polarized mesons, it seems that their experimental measurement is out of the question.

Corrections to the denominators in the expression of the amplitude contribute only at $O(m^2/Q^2)$, and may generally be neglected. However, we must consider their effect on the endpoint behavior in z and y.

The former is fairly simple. The upper bound $z_{\max}$ on z is determined by our assumption of duality; if the mass of the hadronizing system, $\overline{\bar{z}}Q$, is too small,

that assumption fails, and our predictions are vulnerable to large corrections from poorly understood resonance physics. For light-quark systems, we require $\overline{\bar{z}}Q > 2$ GeV [27]. For systems containing a single heavy quark, we should then require $\overline{\bar{z}}Q > m_{\mathbf{q}} + 2$ GeV, decreasing the upper limit $z_{\max}$.

The kinematic limit on the back momentum y_1 of the heavy (anti)quark is then $y_1 > m_{\mathbf{q}}^2/\bar{z}Q^2$. The *prima facie* effect of this limit is simply to excise a region of the cross section. However, more careful consideration shows that the interplay between $m_{\mathbf{q}}$ and y_1 also affects the experimental acceptance; we will return to this point in Section 7.4.

3.2 Non-valence Fock states

This is the greatest technical challenge we must face. The difficulty arises from the fact that the regulation of infrared divergences in inclusive processes relies on the cancellation between graphs like those of Figs. 8(a) and (b); however, when we demand that the collinear final-state particles form a meson, we risk spoiling this cancellation.

In the consideration of exclusive production in the valence state, the incomplete cancellation of infrared divergences leads to the 'Sudakov suppression' of exclusive production [7,26,28]. The Sudakov form factor for exclusive production of a bare colored particle vanishes in the absence of an infrared cutoff. However, in production of color-singlet states the transverse size of the hadron itself provides a natural infrared cutoff, rendering the Sudakov form factor finite.

Our aim, then, is to compute the contribution from $q\bar{q}g$ Fock states, which correspond to infrared-divergent hard-scattering amplitudes, in a manner consistent with the existing treatment of Sudakov effects. To this end, we consider

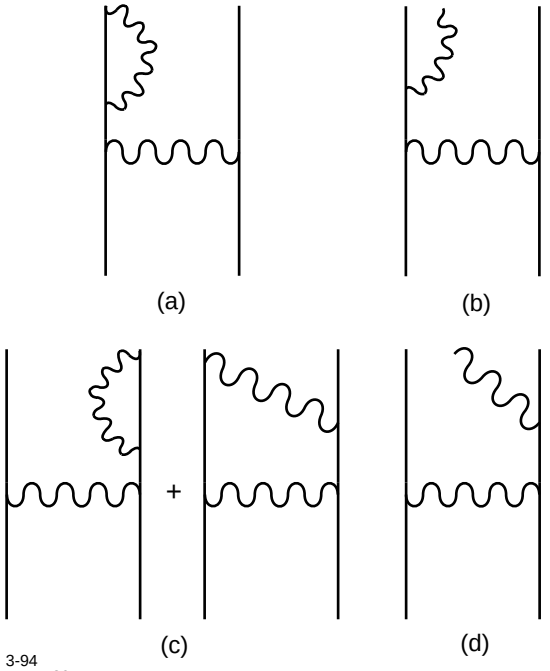

Figure 8. Diagrams which cancel to provide infrared-finite predictions for inclusive amplitudes. (a) shows a higher-order correction to the process of Fig. 1; (b) shows a diagram whose collinear divergence cancels against that of (a). In exclusive production, we must consider the diagrams of (a) and (c) to obtain the Sudakov-corrected amplitude for color-singlet production. The factorization prescription, meanwhile, tells us that (b) and (d) are to be excluded from the hard-scattering calculation (but see Fig. 9(b)).

the prescription of Ref. [1] for the calculation of exclusive amplitudes. In the graphs of Figs. 8(b) and (d), let $k_\perp$ denote the gluon's transverse momentum with respect to the hadron direction of motion. If $k_\perp^2$ is smaller than the factorization scale Q^2, we are required to absorb these (possibly nonperturbative) terms into the bound-state dynamics, rather than compute them in pQCD. Conversely, if $k_\perp^2 > Q^2$, the gluon is no longer sufficiently collinear to be included in the distribution amplitude defined in Eq. (1.2). Thus we should consistently drop contributions from all such diagrams. One might worry that the remaining sum of diagrams will lack gauge invariance; however, we have verified by explicit computation that the diagrams thus discarded become gauge-invariant in the collinear limit.

Figure 9 shows the Feynman diagrams we must evaluate to compute the amplitude for production in the one-gluon Fock state. These diagrams possess no collinear divergences, and their calculation is straightforward. We obtain the hard-scattering amplitude

$$\begin{aligned} T_H^{(+)} = \frac{c^2}{z\ \overline{y_1 y_2}}\ & \frac{q_s y_1}{\bar{x}_1 x_2 (1-z x_1) y_2} - \frac{q_u y_2}{x_1 \bar{x}_2 (1-z x_2) y_1}\ \times \\ & \times\ \ C_1(\bar{z}+z x_3) + C_3(\bar{z}+2 z x_3) \\ & + C_2 s c e^{i\phi}\ \ \overline{\bar{z}}\ \frac{q_s}{x_2(1-z\bar{x}_2)y_2} - \frac{q_u}{x_1(1-z\bar{x}_1)y_1} \end{aligned} \tag{3.3}$$

for production of pseudoscalar or of longitudinally polarized vector mesons. The color factors $C_1 = -1/3\ \ \overline{3}$, $C_2 = 8/3\ \ \overline{3}$, and $C_3 = i\ \ \overline{3}$ correspond to the diagrams of Figs. 9(a), (b), and (c), respectively.

Like the helicity-violating amplitudes of the previous section, the amplitudes for production in a non-valence state can best be measured in regions where leading-twist production is forbidden. Thus we again consider the production of transversely polarized vector mesons. The full hard-scattering amplitude is quite awkward; however, since we are interested in production with a $\sin^2\theta$ angular distribution, we present only the part proportional to $\sin\theta$:

$$\begin{aligned} \tilde{T}_H^{(+)} = \frac{e^2 g_s^3}{Q^3}\ \ \overline{\bar{z}} \Bigg\{ & -\frac{C_1 q_u}{x_1(1-z\bar{x}_1)}\frac{y_2}{y_1} + \frac{C_3 q_s}{z\bar{x}_1 x_2}\ \frac{1}{y_1} - \frac{z+y_1}{z y_2} + \frac{1}{1-z x_1} \\ & + \frac{2C_2}{z^2}\left(\frac{q_s}{x_2 y_2}\ \frac{1}{x_3\bar{x}_3} - \frac{y_1}{\bar{x}_1}\ - \frac{q_u}{x_3}\ \frac{1-z x_3}{x_1\bar{x}_3} + \frac{y_2}{\bar{x}_2 y_1}\ \right) \Bigg\}. \end{aligned} \tag{3.4}$$

Again, no numerically large coefficients appear. While the gluon is expected to carry less average momentum than the quarks, the distribution amplitude is suppressed by x_3^2 as $x_3 \to 0$, because a very soft gluon cannot couple to a singlet $q\bar{q}$

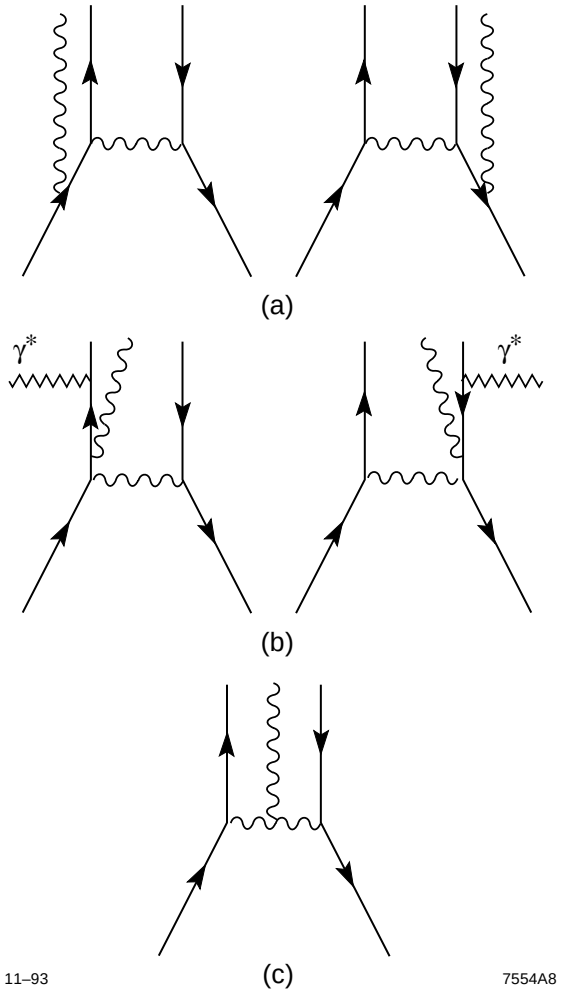

Figure 9. The Feynman diagram topologies which must be included in the amplitude for production of a meson in a $q\bar{q}g$ Fock state. In (a) and (c), a sum over all possible attachments of the γ^* is implicit. In (b), however, only the specific attachment shown should be used; the rest are considered in Figs. 8(b) and (d).

state. Thus $\left\langle x_3^{-1} \right\rangle$ is not extremely large. Also, in this case the suppression factor is μ/Q, where $\mu \lesssim 0.5$ GeV does not depend on quark masses; thus higher-twist contribution to the cross section will probably be invisibly small. To proceed further, we need information about the distribution amplitude $\phi_{h \to q\bar{q}g}$; this is the subject of the next section.

3.3 Non-valence distribution amplitudes

In order to estimate the size of the contribution to the semiexclusive cross section from the higher-twist terms of the preceding section, we must have some model of the meson distribution amplitudes for the non-valence states in question.

One approach to this problem is undertaken by Zhitnitskiĭ *et al.* [29], who extend the sum-rule approach of Refs. [13–15] to wavefunctions of nonleading twist.

They propose model distribution amplitudes for the $q\bar{q}g$ states of the π and ρ: we are interested in the distribution $\phi_{3\rho}^V$ of transversely polarized ρ mesons [30]. The sum-rule model distribution is

$$2520 f_{3\rho} x_1 x_2 x_3^2 (x_1 - x_2)(7 - 15 x_3), \tag{3.5}$$

where $f_{3\rho} \simeq 3.5 \cdot 10^{-3}$ GeV^2; thus, when convolving the hard-scattering amplitude and distribution amplitude, we must replace

$$\frac{1}{\bar{x}_2 x_3} \to -14 f_{3\rho}, \qquad \frac{1}{\bar{x}_1 x_2} \to 28 f_{3\rho}, \qquad \text{and} \quad \frac{1}{x_2 x_3 \bar{x}_3} \to 35 f_{3\rho} \simeq 0.12 \text{ GeV}^2. \tag{3.6}$$

Thus the extreme smallness of $f_{3\rho}/Q$ more than counterbalances the numerical enhancement from the factors of x_i in the denominator.

Comparison of Eqs. (3.2) and (3.4)–(3.6) suggests that, in light mesons, quark mass effects are more important than effects from non-valence Fock states for $m_{\mathbf{q}} \gtrsim 700$ MeV. Of course, this is an extremely rough estimate. However, for our purposes it is sufficient to demonstrate that production in non-valence Fock states does not provide a measurable signal.

We can compute the corrections of order μ/Q resulting from our neglect of Fock states with nonzero orbital angular momentum by including a small transverse momentum $\pm\epsilon_\perp$ in the spinors $u_\pm(p)$ of Appendix A. Specifically, we wish to consider the contribution from hard scatterings like $e^+e^- \to s_-\bar{d}_- X \to K_L^* X$.

The wavefunction must carry a unit of orbital angular momentum, in order to offset the difference in the spin states of the meson and of its quark constituents. Thus the moment of $\epsilon_x + i\epsilon_y$, and with it all such terms in the amplitude, vanishes, while $\epsilon_x - i\epsilon_y$ may be replaced with some typical transverse momentum μ.

For example, the term of order μ/Q and proportional to $\sin\theta$ in the amplitude for semiexclusive production of longitudinally polarized K^* mesons is

$$sce^{-i\phi} \quad \frac{}{\bar{z}} \; \frac{xq_s}{\bar{x}(1-zx)y_2} - \frac{\bar{x}q_d}{x(1-z\bar{x})y_1} \quad . \tag{3.7}$$

Neglecting the factor μ/Q, this is numerically smaller than the corresponding term in Eq. (3.2); thus the error which its neglect introduces into our calculations is negligible, while the chance of measuring its contribution separately is remote.

4. Transverse momentum, Sudakov effects, and the running coupling

So far, we have neglected the running of the strong coupling constant α_s. While this is technically a correction at next-to-leading logarithmic order, it assumes

great importance in exclusive reactions because of the divergence of the one-loop running coupling

$$\alpha_s(Q^2) \equiv \frac{4\pi}{\beta \ln(Q^2/\Lambda^2_{\rm QCD})}$$

as $Q^2 \to \Lambda^2$.

It is our belief that too much has been made of this divergence, which stems from an extrapolation using the lowest-order (one-loop) QCD β function into precisely that region in which the lowest-order approximation is invalid. Nonetheless, in the absence of a better form, one would be obliged to use this coupling. The recent work of Mattingly and Stevenson [31] suggests that there is, indeed, a better form; we shall return to this point in Section 5.1.

The soft divergence of α_s affects the computation of exclusive amplitudes even at large momentum transfer, because the gluon virtuality can still be small near the endpoints $x \to 0$, $x \to 1$. In a proper higher-order treatment, we would use a scale-setting procedure, such as BLM [32], to fix the argument of the running coupling α_s through the entire process. However, this is not satisfactory for our purposes for two reasons.

The first and most concrete is that the scale can only be set to given order in α_s when the perturbative coefficients have been obtained to one higher order. Thus no scale-setting is possible when only a tree-level amplitude has been computed, as is the case here.

The second objection is more fundamental: since the momentum transfer through the internal gluon depends on the hadron's distribution amplitude, a single scale cannot consistently be set for all possible distributions. Instead, the model wavefunction enters into the scale, resulting in a formula of redoubled complexity.

This is a true physical effect, not an artifact of the procedure; for example, a wavefunction which is very strongly suppressed at the endpoints will certainly yield a larger mean value of q^2 than will one which is concentrated there.

Thus we must allow the argument of α_s to depend on the momentum fraction x in the hard-scattering process. At first glance, this seems to threaten the finiteness of our results. However, the work of Sudakov and of Mueller [26] demonstrates that exclusive amplitudes remain finite.

Heuristically, the picture is as follows: the coupling can only grow large when the gluon propagates for a large distance (of order $\Lambda_{\rm QCD}^{-1}$) in transverse position space. In this case, the constituents of the final-state hadron are widely separated and have a large color dipole moment. Thus the probability that they will emit final-state radiation, in which case the process is *ipso facto* not exclusive, approaches 1.

Mueller [26] derived the quantitative effects of this Sudakov suppression to leading logarithmic order, and Botts and Sterman [28] extended them to next-to-leading order (in $\ln Q$). We do not wish to use the entire machinery thus derived, but instead will take the low road, absorbing the leading effects of Sudakov suppression into an effective coupling constant $\alpha_{\rm eff}$.

To incorporate Sudakov suppression into the calculation of exclusive amplitudes, we must undo the simplification of Eq. (1.3). However, we use the wavefunction and propagator not in momentum space, but in the hybrid space of longitudinal momentum and transverse position:

$$\frac{\alpha_s(q^2)}{q^2} \to \frac{1}{\pi} \int {\rm d}^2 b \; K_0(b|q|)\alpha_s(q^2), \tag{4.1}$$

where K_0 is a modified Bessel function. The form of Eq. (1.2) is regained if we assume that the wavefunction is independent of b (*i.e.*, that it is proportional to $\delta^2(k_\perp)$). Here and in the following, we assume that q is a purely longitudinal momentum (otherwise see Ref. [7]).

When q^2 is small the proper argument of α_s is not q^2, but rather $\max\{q^2, b^{-2}\}$: the coupling cannot grow large if the gluon propagates over only a short distance [33].

The form of the Sudakov suppression given by Botts and Sterman [28] vanishes as $|b| \to \Lambda^{-1}$ sufficiently rapidly to contain the divergence of α_s in the same limit. For $q^2 > \Lambda^2$, the effect of Sudakov suppression is expressed by the substitution

$$K_0(b|q|)\alpha_s(q^2) b \, \mathrm{d}b \to \int_0^{\Lambda^{-1}} e^{-S(b,q)} K_0(b|q|)\alpha_s\big(\max\{q^2, b^{-2}\}\big) b \, \mathrm{d}b, \qquad (4.2)$$

where $S(b,q)$ diverges as $b \to \Lambda^{-1}$. The contribution from the region $b > \Lambda^{-1}$ in Eq. (4.1) is in any case suppressed by e^{-q^2/Λ^2}, so the main effect for substantial q^2 is the correction to α_s for very small b (which contributes at $O(1/\ln q^2)$ to the amplitude).

For small q^2, the problem is much thornier; the quantitative behavior of the Sudakov suppression comes into play. We take advantage of the fact that the factor $\alpha_s(b^{-2})$ which enters into the tree-level amplitude as computed by Eq. (4.1) is precisely the same as the coupling α_s which controls final-state radiation and leads to the Sudakov suppression, and use in place of Eq. (4.2) the *ansatz*

$$\int_0^{\Lambda^{-1}} \min_{b' \le b} \; K_0(b'|q|)\alpha_s\big(\max\{q^2, b'^{-2}\}\big) \;\; b \, \mathrm{d}b \equiv \frac{\alpha_{\mathrm{eff}}(q^2)}{q^2}. \qquad (4.3)$$

That is, we postulate that the physical amplitude for exclusive processes does not increase with b and use that assumption to derive a finite form for the effective gluon propagator. In fact, since $K_0(x)$ diverges only logarithmically as $x \to 0$, this formula yields

$$\alpha_{\rm eff}(q^2) \sim \frac{q^2}{2\Lambda^2}\frac{4\pi}{\beta \ln(\Lambda^2/q^2)} \qquad \text{as } q^2 \to 0;$$

the finite size of hadrons means that the amplitude for exclusive production increases more slowly than $1/q^2$ for small q^2.

This procedure requires some justification. Our reasoning is that the exclusive production amplitude should not increase with increasing transverse size, as demonstrated in the observation of color transparency [34]. At large q^2, where the Sudakov suppression is well understood, our method reproduces the results of Refs. [26,28] to leading order in $\ln q^2$. Thus we are willing to accept its predictions in the comparatively poorly understood region of small q^2, where the results of Ref. [28] are themselves subject to substantial parametric uncertainties [35].

Finally, this method offers striking ease of computation. Equation (4.3) can be integrated numerically to obtain the values of $\alpha_{\rm eff}$ at all q^2. The result is shown in Fig. 10. The only parameter involved in the determination of $\alpha_{\rm eff}$ is $\Lambda_{\rm QCD}$ itself. Unfortunately, this parameter is not yet well determined; current experimental results give

$$\Lambda^{(3)}_{\overline{\rm MS}} = 318^{+58}_{-51}\ \text{MeV}.$$

The resulting uncertainty in our cross sections is 15%, which is numerically equal to the uncertainty in $\alpha_s(Q = 3\ \text{GeV})$: that is, the Λ-dependence of the cross section does not reflect a sensitivity to soft physics, but an imprecision in the size of the QCD coupling at moderate momentum transfer.

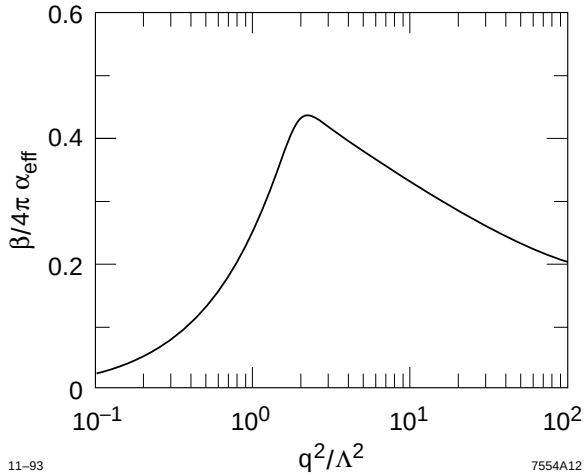

Figure 10. The effective coupling constant $\alpha_{\rm eff}$ as a function of the gluon virtuality q^2.

It must be emphasized that the effective coupling $\alpha_{\rm eff}$ has no applicability outside the domain of exclusive or semiexclusive reactions, since its finiteness results from the finite transverse size of hadrons. It could be argued that we have underestimated $\alpha_{\rm eff}$ by ignoring the possibility that the final-state radiation might be absorbed into the hadron, thus preserving the exclusivity of the reaction; however, such an effect involves the intrinsically soft process of long-distance hadronization, and the events resulting from it will share the characteristics of soft events, rather than of the hard direct processes in which we are interested. Thus we regard such a contribution not as an additional component of the signal, but as a part of the background which should be amenable to calculation with standard Monte Carlo techniques. Also note that the vanishing of the effective coupling, which seems strongly counter-intuitive, is in fact simply a restatement of the fact that the effective propagator diverges less slowly than $1/q^2$ for small q: clearly, the same result is obtained in methods using intrinsic transverse momentum smearing or an artificial gluon mass.

The latter technique is commonly used in the computation of spacelike scattering amplitudes, since an effective gluon mass regulates the divergence of the propagator [36]. This is intended to model the physical effects of the intrinsic transverse momenta within the hadron, which serve to eliminate collinear divergences. We could extend the same approach to the timelike process under consideration, though an imaginary gluon mass would be required. A more accurate treatment could be achieved by inserting a term representing the transverse distribution of the wavefunction [7],

$$\psi_x(k_\perp) \equiv \frac{\psi(x, k_\perp)}{\phi(x)},$$

into the integration of Eq. (4.1), again obtaining an effective coupling which will vanish as $q^2 \ln q^2$ at small longitudinal momentum transfer.

In practice, however, hadronic amplitudes are insensitive to the transverse wavefunction. This is especially true when the Sudakov suppression, which forces the hadron to be formed at small impact parameter, is also considered [7]. Thus we do not expect intrinsic transverse momenta to have a great effect on our results.

In order to test the sensitivity of our results to our assumptions about the effective coupling, we also computed the cross sections with the effective coupling

$$\alpha_s = \frac{4\pi}{\beta \ln (Q^2 + m_g^2)/\Lambda^2}, \tag{4.4}$$

where $m_g = 1.2\,\Lambda$ was chosen to match the value

$$\lim_{q^2 \to 0} \alpha_s(q^2) = 0.82$$

obtained by Mattingly and Stevenson [31,37]. The predicted cross sections at $\overline{s} \simeq 10$ GeV differed by less than 10%, illustrating the relative insensitivity of semiexclusive production to the niceties of soft physics.

5. Higher-order corrections

Before we can have faith in the results we have derived thus far, we must know whether they will be overwhelmed by $O(\alpha_s)$ corrections. We begin by classifying all such corrections.

The first-order corrections to the production mechanism of Fig. 1 are obtained by attaching an additional gluon line to the hadronic topology. Some of the ways in which it may be attached are familiar and have already been dealt with in other contexts.

For example, the higher-order corrections of Fig. 11(b) are precisely analogous to those which modify the total cross section $\sigma_{\rm tot}(e^+e^- \to \text{hadrons})$, since they are completely internal to the color-singlet recoil system. Thus we can, with no calculation whatsoever, be assured that their entire effect is to increase the total measured cross-section by a factor $(1 + \alpha_s(\bar{z}Q^2)/\pi)$ [38].

Similarly, the diagrams of Fig. 11(c) are the same as those which contribute to the study of purely exclusive processes. When the internal gluon momentum q is small compared to the momentum scale Q of the hard process, it may be considered internal to the meson and treated as a correction to the wavefunction.

This brief catalog leaves only two cases uncovered. First, differentiation between diagrams like that of Figs. 11(b) and (c) is not perfectly well-defined, and there will be cases where $q \sim Q$. However, the resulting corrections are suppressed

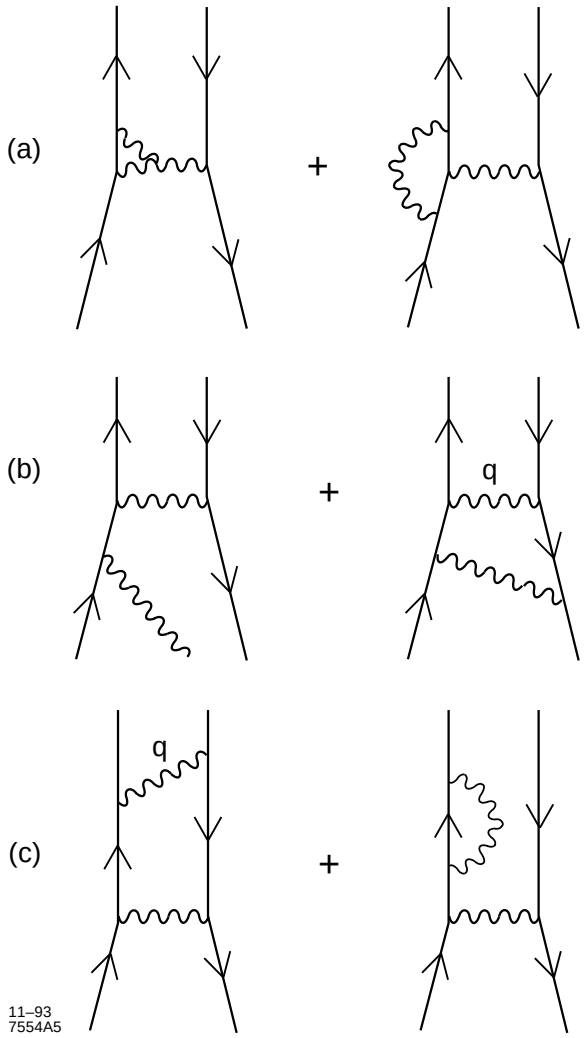

Figure 11. Some diagrams which will yield $O(\alpha_s)$ corrections to the amplitude. (a) is simply a vertex correction. (b) is familiar, when $q^2 \sim Q^2$, from the analysis of inclusive production. (c), with $q^2 \ll Q^2$, is 'factorizable' – internal to the meson – and will have the same effect here as in exclusive processes.

by $\log(Q^2/\mu^2)$ relative to those in which one of the gluon momenta is soft, and we may safely ignore them in this work.

Second, there are unfactorized soft contributions like that shown in Fig. 12. As described in Ref. [28], these give rise to the Sudakov suppression of exclusive amplitudes; the same suppression applies in the semiexclusive case, and we considered its effects in Section 4.

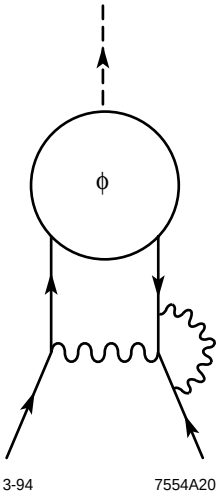

Figure 12. Non-factorizable soft contributions to the hard-scattering amplitude T_H, which lead to Sudakov suppression.

5.1 The infrared-stable coupling

In a recent paper [31], Mattingly and Stevenson show that the third-order corrections to $R_{e^+e^-}$ [39] lead, through the use of perturbation theory optimized with the PMS scale-setting method [40], to a form of the coupling which approaches a constant limit as $q^2 \to 0$. A fit to experimental data on $R_{e^+e^-}$ yields a limiting value $\alpha_s(q^2 \to 0) \simeq 0.82$.

Thus we may choose to adopt a more conservative approach than that described in Section 4, and merely use the coupling of Ref. [31] throughout our numerical calculation [37]. In actuality, neither approach is perfectly satisfactory. The suppression of the effective coupling due to the finite size of hadrons is a physical effect, which the naive insertion of α_s into exclusive amplitudes ignores; but the form of Ref. [28] for the Sudakov suppression is partly predicated on the low-q^2 divergence of the coupling, and is now subject at least to quantitative revisions which are outside the scope of this paper.

In practice, the use of $\alpha_{\rm eff}$ has the virtue that it naturally incorporates Sudakov effects which serve to contain the collinear (small-y_i) divergence that appears in the tree-level amplitudes of Eqs. (2.6) and (2.7), and to improve the numerical behavior near the endpoints. The physics of this apparent divergence and the means by which the correct endpoint behavior may be computed are the subjects of the next chapter.

6. The small-y collinear divergence

The tree-level amplitudes of Eqs. (2.6)–(2.11) diverge for $y_i \to 0$, as the internal gluon approaches its mass shell. This apparent divergence is in fact controlled by several corrections which become important in this limit. We will discuss some of them, in order of importance.

6.1 Wavefunction vs. distribution amplitude

The factorization of Eq. (1.2), which assumes that T_H depends only weakly on the internal momenta $k_\perp$, is clearly invalid when the momentum transfer $y_i Q^2$ of the exchanged gluon becomes comparable to a typical hadronic momentum scale μ^2.

At this point, we must undo the factorization used in Eq. (1.3), and instead consider diagrams like those shown in Fig. 13. In this region, the diagram of Fig. 13(b) is suppressed by a factor of y_i relative to that of Fig. 13(a) and may safely be neglected. The amplitude may then be evaluated in terms of the quark fragmentation amplitude $\psi_{q\to hQ}$. To leading order in y_i, we obtain

$$\mathcal{M}^{(+)} = e^2 q_i C_F \, c^2 \psi_{q\to hQ}(z, j_\perp), \qquad \text{where} \quad j_\perp^2 = z^2 \bar{z} y_i Q^2,$$

the color factor $C_F = \quad \overline{3}$, and q_i is the QED charge of the quark q.

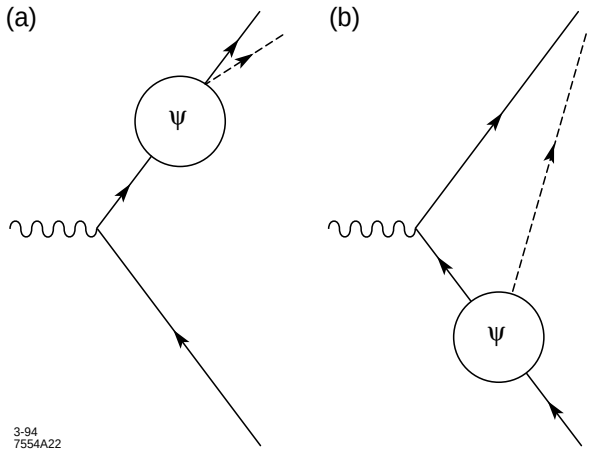

Figure 13. The diagrams contributing to the semiexclusive production amplitude at small y_1. (a) shows the leading-twist part (in physical gauges), (b) a higher-twist part.

Thus

$$\int_0^{y_{\rm crit}} \mathrm{d}y_1\ |\mathcal{M}^{(+)}|^2 = 3e^4 q_i^2\, c^4 \int_0^{zQ\sqrt{\bar{z}y_{\rm crit}}} \frac{\mathrm{d}^2 j_\perp}{\pi z^2 \bar{z} Q^2} |\psi(z, j_\perp)|^2 = \frac{768\pi^4 \alpha^2 q_i^2}{z^2 \bar{z} Q^2}\, c^4 \tilde{g}_{h/q}(z; zQ \quad \overline{\bar{z}y_{\rm crit}}), \tag{6.1}$$

where

$$\int^{Q_0} \frac{\mathrm{d}^2 k_\perp}{16\pi^3} |\psi(x, k_\perp)|^2 \equiv \tilde{g}_{h/q}(x; Q_0) \leq G_{h/q}(x; Q_0);$$

here $G_{h/q}(x)$ is the fragmentation function for finding a meson h inside the quark q at momentum transfer Q_0. The full fragmentation amplitude G differs from $\tilde{g}$ in that G includes a sum over all Fock states, while $\tilde{g}$ receives a contribution only from the exclusive 'decay' $q \to hQ$. At large z, however, this difference should vanish; it is expected that the valence Fock state dominates the structure and fragmentation functions at large x.

Combining Eqs. (6.1) and (2.1), we find that the total spin-averaged contribution to the cross section from the region $y < y_{\rm crit}$ is

$$\mathrm{d}\sigma = \frac{3\pi\alpha^2 q_i^2}{8zQ^2}\tilde{g}_{h/q}(z; zQ \quad \overline{\bar{z}y_{\rm crit}})(1+\cos^2\theta)\mathrm{d}\cos\theta\,\mathrm{d}z. \tag{6.2}$$

We have integrated out the trivial ϕ-dependence.

Several things about the contribution to the cross section given by Eq. (6.2) are noteworthy. First, and most disturbing, it is leading-twist; the suppression of the cross section is only Q^{-2}. Thus we must take great care to separate the higher-twist direct production in which we are interested from this 'direct fragmentation' contamination.

That this is possible at all is due to the nature of the hadronization process. At high energies, where the extra Q^{-2} suppression of the semiexclusive signal is severe, the jets inherit the parton momenta; thus the small-y region can be identified and discarded with great accuracy. In order to pass cuts designed to ensure that the meson is produced with a high degree of isolation, the events described by Eq. (6.2) must be transformed in the hadronization process into events in which no jet is near the meson; the probability that this will occur is suppressed by Q^{-2} for large Q. The leopard can change his spots, but it requires an intrinsically higher-twist process. Thus the signal for semiexclusive production at moderate y_i is in principle measurable even at arbitrarily large Q^2.

In fact, the signal from the collinear region which passes the event shape cuts resembles a higher-order correction to the tree-level semiexclusive signal. To see this, recall that a hard gluon must be exchanged between the quark and antiquark in the recoil system, so that jets will not form near the meson. Adding this gluon to the tree-level diagram of Fig. 1, we get the diagram of Fig. 11(c); the soft gluon

which appears in near-collinear tree-level production corresponds to a soft gluon internal to the meson in the more complete picture.

Two complications, however, prevent us from lightly discarding the collinear region from consideration. First, many interactions can take place between the near-collinear quark and meson, rather than the single gluon exchange which appears in the perturbative computation. Second, the momentum transfer between the outgoing quark and antiquark also need not be carried by a single gluon, since we do not demand exclusivity and are unable to completely specify the final-state momenta. As a result, such contributions lack a perturbatively calculable hard scattering and must be treated by Monte Carlo techniques.

To estimate the contribution to the measured semiexclusive cross section, we need to model the fragmentation function $\tilde{g}$. Since we are interested in the region of large z, we will assume

$$\tilde{g}(z) = G(z); \tag{6.3}$$

this is a somewhat pessimistic but not inaccurate assumption. The structure functions $G(x)$ near $x = 1$ are expected to have the form

$$G(x; Q^2) = C(1-x)^2 + \frac{D}{Q^2},$$

where C is a dimensionless constant parametrizing the leading-twist behavior, and D represents higher-twist terms [41]. The approximate forms

$$G_{\pi^+/u}(x) = G_{\pi^-/d}(x) = 1.54(1-x)^2 \qquad \text{and} \quad G_{\pi^-/u}(x) = G_{\pi^+/d}(x) = 0.54(1-x)^2$$

fit the experimental observations [42] within statistical errors. We are not interested in the higher-twist corrections, which share the Q^{-4} behavior of the

semiexclusive signal and will make a negligible contribution to the signal after experimental cuts.

Thus, summing over quark and antiquark flavors and assuming $SU(3)$ symmetry, we obtain the estimate

$$\mathrm{d}\sigma = C_h \frac{\alpha^2}{Q^2} \frac{\bar{z}^2}{z} \mathrm{d}z \; (1 + \cos^2\theta) \mathrm{d}\cos\theta, \tag{6.4}$$

where $C_h = 1.50$ for π and $K^{\pm}$, and $C_h = 1.11$ for K^0 and $\bar{K}^0$. This is not a small effect, but rather comprises a substantial fraction of all events!

Since the backgrounds of this sort are so substantial and involve no short-distance physics in the jet formation process, we expect that they will be well simulated by Monte Carlo models. Thus we defer further analysis of this region to Section 7, where we will examine hadronization effects. We will see that a judicious combination of experimental cuts can reduce the contamination from the endpoints to acceptable levels.

6.2 Multiple scatterings and y_{crit}

To accurately predict the rate of semiexclusive production, we must obtain a good estimate of the value y_{crit} at which the factorization of Eq. (1.3) is no longer reliable.

Let us consider the physical picture of direct pQCD production, shown in Fig. 14. Semiexclusive production depends on the hadron's undergoing no final-state interactions, and this can only proceed if the quark interacts with the antiquark before scattering from the hadron.

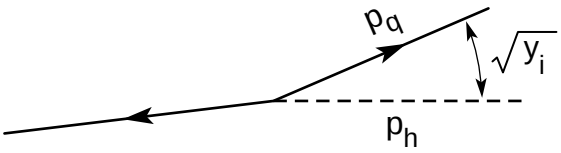

Figure 14. The physical picture of direct meson production at leading order. Final-state interactions are more likely between particles which emerge in close proximity.

Thus we parametrize the rates A_h and $A_{\bar{q}}$ for the quark to interact with the hadron and antiquark, respectively. Neglecting for the moment the running of the coupling strength, we obtain

$$\frac{A_h}{A_{\bar{q}}} = \frac{\bar{z}^2\mu^2}{z^2 y_2^2 Q^2} \qquad \Rightarrow \quad y_{\rm crit} \simeq \frac{\bar{z}}{z}\Big(\frac{\mu}{Q}\Big); \tag{6.5}$$

the factor of μ^3/Q^2 comes from comparison of the $1/r^2$ behavior of the interactions between nonsinglet particles to their $1/r^4$ 'tidal' interactions with singlet particles [43]. As Q increases, the degree of collinearity of the meson constituents increases, and $y_{\rm crit}$ must decrease. Including the running of the QCD coupling would decrease this estimate somewhat, but since the energy of the qh system grows as a power of Q, the behavior given in Eq. (6.5) will still hold.

The wavefunction of Fig. 13 takes into account all such multiple scatterings; $G_{h/q}(z)$ should be interpreted as the amplitude for the hard probe from the recoil antiquark to find the quark in a qh state. Thus the prediction of Eq. (6.2) is unaffected by multiple hard scatterings, as long as the assumption of Eq. (6.3) holds.

For $y > y_{\rm crit}$, the squared invariant mass of the qh system is at least $zy_{\rm crit}Q^2 \simeq \bar{z}\mu Q \gg \mu^2$, so that once multiple scattering occurs the probability of finding the

original qh system again in a qh state may be neglected. Thus we account for the possibility of multiple scattering for $y > y_{\rm crit}$ by including a suppression factor

$$\frac{A_{\bar{q}}}{A_h + A_{\bar{q}}} = \left(1 + \frac{y_{\rm crit}^2}{y^2}\right)^{-1}. \tag{6.6}$$

6.3 Other soft corrections

Other intrinsically soft processes will affect the behavior of the amplitude near the collinear pole. For example, terms proportional to the intrinsic transverse momenta will be less thoroughly suppressed, so that formation in Fock states with $L_z \neq 0$ will proceed with probability $\mu/y_{\rm crit}Q$; however, this is still a small number, scaling as $Q^{-1/2}$. Since we will see that our experimental cuts effectively exclude the small-y region, we do not consider this possibility further.

The finite size of hadrons, as enforced by Sudakov suppression [7,26,28,44], where the tendency of large color dipoles to emit final-state radiation suppresses the effective wavefunction at large impact parameter b, has been dealt with in Section 4. The conclusions reached there are certainly invalid at the collinear pole itself, however, since the process by which the hadron is formed is itself soft. Indeed, the result of Eq. (6.2) implicitly accounts for all soft corrections by absorbing them into the measured fragmentation function. However, Sudakov effects should be important for $y_i > y_{\rm crit}$; we will return to this point in the next section.

6.4 Sensitivity to $y_{\rm crit}$

Our focus will be on finding experimental cuts which isolate the 'good' region $y > y_{\rm crit}$ from the dangerous region in which multiple scattering becomes important. We must, however, be able to estimate the contribution from the small-y endpoints, so that we may be sure that our predictions are trustworthy.

We have now dealt with the region $y < y_{\rm crit}$ unambiguously, and have found that standard Monte Carlo techniques should represent it accurately. One difficulty remains: the sensitivity of our results to $y_{\rm crit}$. Clearly, in a correct treatment which accounts properly for the contributions from all values of y, the precise value of $y_{\rm crit}$ should be irrelevant. However, this is far from the case here—since the differential cross section from Eq. (2.6) diverges like y_i^{-2}, we may see a power-law dependence on $y_{\rm crit}^{-1} \sim Q/\mu$ in our results.

What physical mechanisms are important in this region? Since the transfer is of order $y_i Q^2 \sim \mu Q$, the process is still perturbative, but approaching the soft region. This is precisely the domain in which Sudakov effects become important [44].

With the effective coupling program implemented in Section 4, we find that the inclusion (albeit in a somewhat naive manner) of Sudakov effects naturally regulates the small-x and small-y divergences of amplitudes like that of Eq. (2.6). While we cannot trust the inherently perturbative mechanisms employed in this derivation in the region $y < y_{\rm crit}$, they should be reasonably accurate in the region $y > y_{\rm crit}$ where the momentum transfer $y_i Q^2$ is large enough to allow a perturbation expansion. Thus in this region the effective-coupling method is insensitive to parametric variations [45]. One feature of this effective coupling is its $q^2 \ln q^2$ behavior at small q^2. Since the gluon virtuality vanishes in the limit $y_i \to 0$ with which we are concerned, use of the effective coupling replaces the $1/y$ divergences of

Eqs. (2.6)–(2.13) with integrable $\ln y$ divergences. However, the numerical behavior at the endpoints is still unfriendly, and depends on the value of $\Lambda_{\rm QCD}$. We will depend on stringent experimental cuts to eliminate the dependence on endpoint behavior, and thus on our treatment of soft physics, of the observed cross sections after integration over y.

7. Hadronization effects

In Refs. [2] and [3], it was assumed that the width of the (angular or rapidity) gap by which the directly produced meson was isolated would be unchanged by the hadronization process; *i.e.*, that the products of hadronization will fill the region of phase space spanned by the free partons, but not spill out of it. We shall see that this naive assumption is highly misleading.

Since we are concerned with the intrinsically soft process of hadronization, we may use a phenomenological model of such processes, the Lund Monte Carlo generator [46].

Most of our attention will be devoted to two cases: $Q \simeq 10$ GeV, where B factories may operate in the near future, and $Q = m_Z$. In the former case we will enforce the condition of isolation by requiring either an angular gap (in the center-of-momentum frame) or a rapidity gap [23] between the candidate directly produced meson and the other products of hadronization; in the latter, we will use isolation in rapidity space exclusively.

7.1 Isolation cuts

The first order of business is to demand a high degree of isolation of the candidate directly produced meson in order to reject backgrounds from inclusive processes. In each case, we used the LUND Monte Carlo generator to model the development of the recoil system. As explained previously, since the hard physics does not influence the hadronization process, we expect such a simulation to be very accurate. We studied the hadronization of $u\bar{u}$ systems with the initial state momenta given by the kinematics of Section 2.

Most of the systems we are interested in are asymmetric systems such as $u\bar{s}$; however, since the dynamics of hadronization are flavor independent, we confidently expect that the errors thus introduced are negligible for light (uds) systems. We will return to the issue of heavy quarks later.

Given the kinematic variables z and y_1, we can define cumulative acceptance functions:

- $P_{\rm ang}(\theta; z, y_1)$ is the fraction of events at given z and y_1 in which the directly produced meson is isolated by a cone of opening half-angle θ in the event center-of-momentum frame;
- $P_{p_z}(p_{\rm cut}; z, y_1)$ is the fraction of events in which no particle except the directly produced meson has $p_z > p_{\rm cut}$ [47]; and
- $P_{\rm rap}(Y_{\rm max}; z, y_1)$ is the fraction of events in which no particle has rapidity greater than $Y_{\rm max}$ along the $\hat{z}$-axis [23,48].

The regions of momentum space excluded by these cuts are shown in Fig. 15. Intuitively, one can see the advantage of the rapidity gap: it is not greatly affected by either soft physics in the same hemisphere or hard physics at large angles.

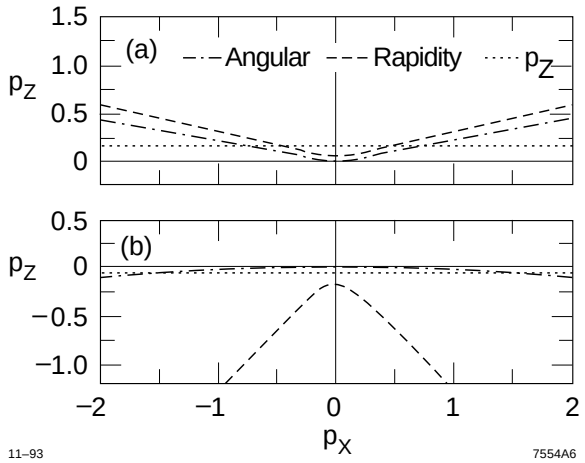

Figure 15. The regions of momentum space excluded by the isolation cuts we consider. The numerical values shown are those used for $Q = 10.58$ GeV and (a) $z = 0.7$, (b) $z = 0.95$. In each case, the isolation cut is given by the requirement that the phase space above the line be empty except for the candidate directly produced meson itself. It must be emphasized that the stringency of the cuts is not a matter of taste, but is chosen to maximize the figure of merit U of Eq. (7.1).

We obtained numerical values for $P(x; z, y_1)$ with the Monte Carlo generator, typically in runs of 20,000 events. We then optimized the cut with the figure of merit

$$U \equiv \frac{\int_0^1 P(x; z, y_1) \mathrm{d}y_1}{P(x; z, y_1 = 0)}. \tag{7.1}$$

This method of optimization is chosen to reflect the fact that the dominant source of background noise is the direct fragmentation contribution of Eq. (6.2). Truly inclusive events are comparatively easy to exclude, especially given the severity of the cuts which maximize U.

Maximizing this figure of merit for each choice of z, we find that the resulting $\theta(z)$ are well described by

$$\cot\theta = \frac{0.370 - 0.438z}{1 - z}. \tag{7.2}$$

Note that the angular isolation is still extreme even at moderate z; for example, we demand that a meson with $z = 0.5$ be isolated by 73°. The stringent cuts are necessary mainly to reduce the background from direct fragmentation, Eq. (6.2).

We also optimized the cuts $p_{\rm cut}$ and $y_{\rm max}$ at each value of z; the results of this optimization agreed well with the fits

$$p_{\rm cut} = (0.70 - 0.79z)\ {\rm GeV} \tag{7.3}$$

and

$$Y_{\rm max} = \frac{0.463 - 0.541z}{1 - z}. \tag{7.4}$$

It is interesting to note that the point at which the angular cutoff is equivalent to the requirement of isolation in a hemisphere ($z = 0.845$) is nearly identical to the corresponding point for the rapidity cut ($z = 0.856$). We will make us of this fact shortly.

The acceptance curves with $Y_{\rm max}$ defined by Eq. (7.4) and those with θ given by Eq. (7.2) are shown in Fig. 16. For moderate z, the rapidity cut is clearly superior to the angular isolation requirement; for large z, however, the rapidity cut is too restrictive, suppressing the signal as well as the small-y noise.

A little thought shows the reason for this. When $z < 0.85$, the situation is as depicted in Fig. 15(a); the rapidity cut is insensitive to very soft physics. For $z > 0.85$, however, the cuts are as shown in Fig. 15(b); now the rapidity cut forces every particle to have some substantial momentum in the $-\hat{z}$ direction. Thus the rapidity cut is more likely to reject semiexclusive events due to soft physics in the hadronization process, and the angular cut is superior.

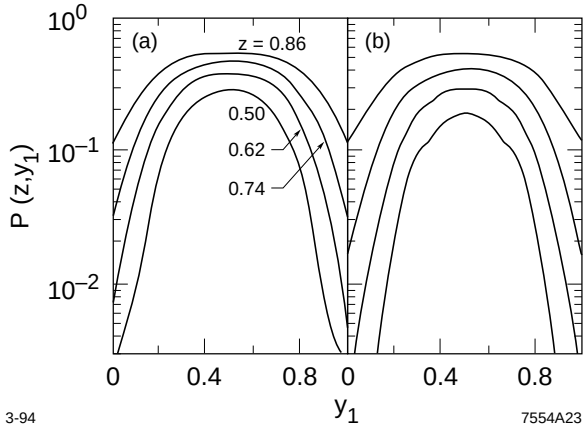

Figure 16. The acceptance $P(z, y_1)$ with (a) the rapidity cut defined in Eq. (7.4) and (b) the angular cut of Eq. (7.2).

With this reasoning, we choose to implement a hybrid cut. For $z < 0.85$, we impose a rapidity cut with

$$Y_{\max} = 0.551 \, \frac{0.85 - z}{1 - z}; \tag{7.5}$$

for $z > 0.85$ we use an angular cut with

$$\frac{x}{\sqrt{1 - x^2}} = -0.429 \, \frac{z - 0.85}{1 - z}. \tag{7.6}$$

This yields the cleanest event sample over the full range of z.

This represents a step towards cleaning up the semiexclusive signal. However, our numerical results (Fig. 17) show that the cuts given so far cannot by themselves adequately restrict the contamination from the small-y region. For this, a further cut is necessary.

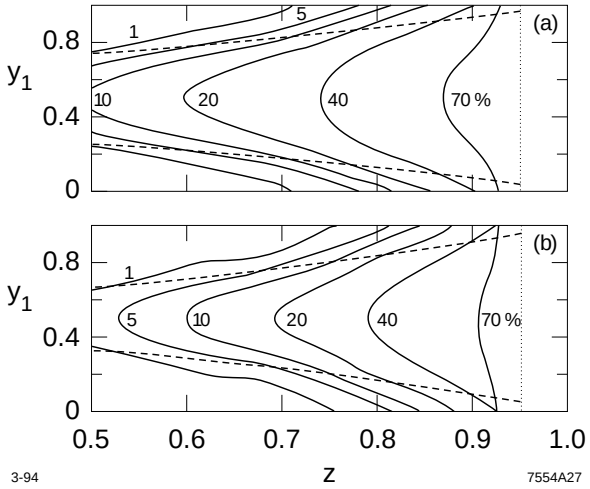

Figure 17. Contours of constant acceptance in the zy_1-plane for $Q = 10.577$ GeV, with the cuts (a) $\cos\theta < 0.172$ and (b) $\cos\theta < 0$, corresponding to 80° and 90° isolation respectively. Dotted lines show the acceptance cuts used in Ref. [3], which are valid in the large-Q^2 limit but at this energy drastically overestimate the acceptance at moderate z.

7.2 Event shape cuts

As described in Section 6.2, events from the small-y region carry their own signature—the jets tend to be aligned with the hadron momentum, which we define to lie along the $\hat{z}$-axis. This allows the isolation cut to preferentially exclude those events to some extent. However, we can improve the discrimination by going directly to the heart of the matter and examining the shape of the hadronizing system.

We first impose a minimum cut on the thrust

$$T \equiv \max_{\hat{n}} \left\{ \frac{\sum_i |p_i \cdot \hat{n}|}{\sum_i |p_i|} \right\} > T_{\min}.$$

Events with low T are somewhat amorphous, and thus carry little information about their original orientation.

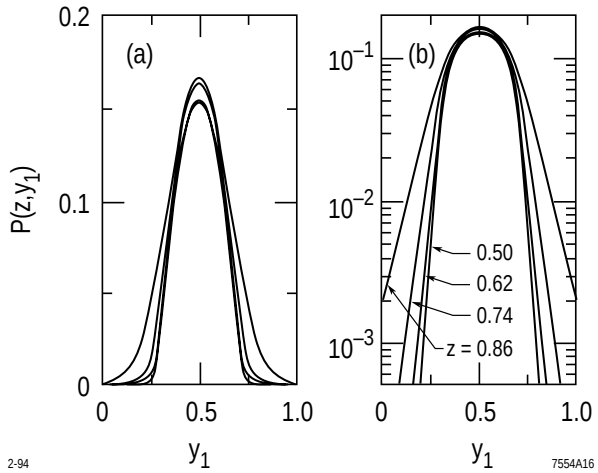

Figure 18. The acceptance $P(z, y_1)$ with the combination of event shape and isolation cuts of Eqs. (7.7) and (7.8): (a) is linear, (b) a semilog plot.

We could attempt to impose a condition on the angle between the thrust axis and $\hat{z}$; however, it turns out to be more efficacious to restrict the 'z-component' of thrust [49]:

$$T_z \equiv \frac{\sum_i |p_i \cdot \hat{z}|}{\sum_i |p_i|} < T_{\max,z}.$$

We again optimized the cuts $T_{\min}$ and $T_{\max,z}$ through numerical evaluation of the figure of merit U. In the end, we found it best to choose the isolation cut

$$Y_{\max} = 0.88 - z, \tag{7.7}$$

and to use the event shape cuts

$$T_{\min} = 0.90 - \frac{0.036}{1-z} \quad \text{and} \quad T_{\max,z} = 0.34. \tag{7.8}$$

To eliminate low-multiplicity inclusive backgrounds, we also required that the recoil system contain at least six particles. The resulting acceptance $P(z, y_1)$ is shown in Figs. 18 and 19. The rejection of small y is now nearly perfect; as a result, we will be able to isolate a clean semiexclusive signal from the region of moderate y.

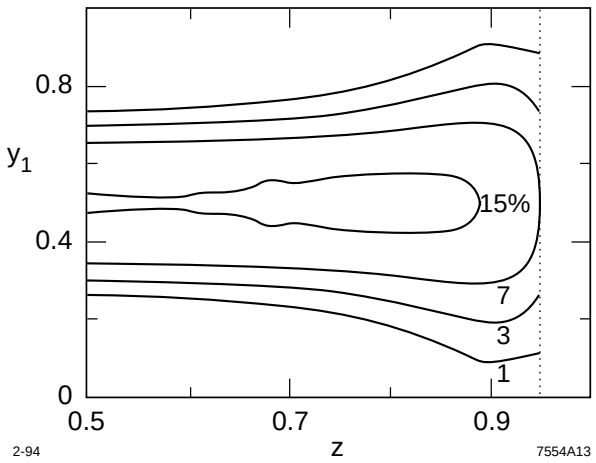

Figure 19. Contours of equal acceptance in the zy_1-plane, with cuts from Eqs. (7.7) and (7.8).

7.3 Acceptances at the Z peak

In precisely the same manner as above, we can define, optimize, and compute acceptances $P(z, y_1)$ at $Q = m_Z$. In this case, we replace Eqs. (7.7) and (7.8) with the requirements

$$Y_{\max} = 1.6 - 1.4z, \quad T_{\min} = 0.90 - \frac{0.004}{1-z}, \quad \text{and} \quad T_{\max,z} = 0.57 - 0.23z. \quad (7.9)$$

Figure 20 shows the results of these constraints. The acceptances are substantially larger in the central region, and much better suppressed at the endpoints in y_i, than the acceptances at $Q = m_\Upsilon$. This serves to offset the increased predominance of the leading-twist collinear contribution, as described in Section 6.1.

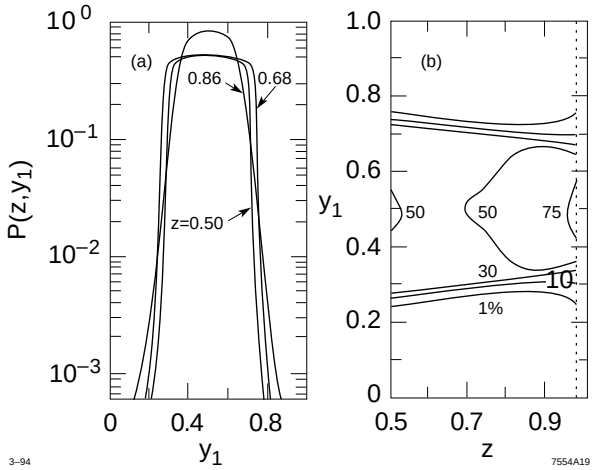

Figure 20. The acceptance $P(z, y_1)$ at $Q = m_Z$, with the cuts of Eq. (7.9): (a) is a semilog plot, (b) a contour plot.

7.4 Quark mass effects

To examine the interesting cases of semiexclusive D production at the Υ resonance and B production at the Z^0 pole, we must allow for nonzero quark masses, and the concomitant energetic weak decays, in the computation of the acceptance $P(z, y_1)$. This does not involve any conceptual changes to the approach we have described; in particular, Monte Carlo simulation of the hadronizing system should still provide physically reliable results.

Figure 21 shows the results of this analysis. Note that the restriction on the mass of the hadronizing system leads to a much more severe constraint on z; otherwise, the results are qualitatively similar to those of Section 7.2.

Similarly, we must account for the B mass and weak decay channels in analyzing the acceptance for B production at the Z peak. Figure 22 shows the results of this analysis; again, the effects of the quark mass are not very large.

At moderate z, the b quark is heavy compared to the scale of hadronization but light enough that its weak decay products are collimated in the direction of its

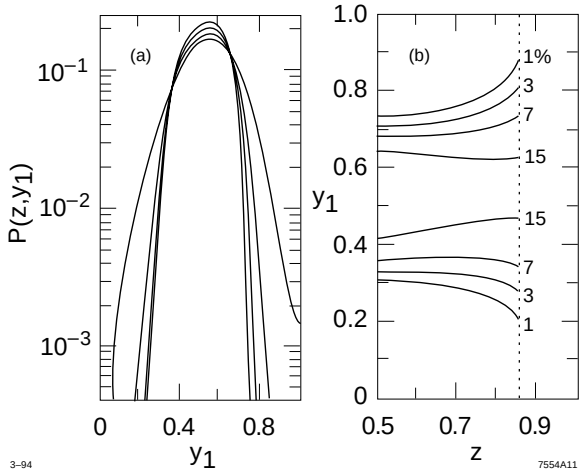

Figure 21. The acceptance $P(z, y_1)$ for semiexclusive production of charmed mesons at the Υ_{4s} resonance. Here $y_1 = y_c$ is the back momentum of the $\bar{c}$ quark in the hadronizing system.

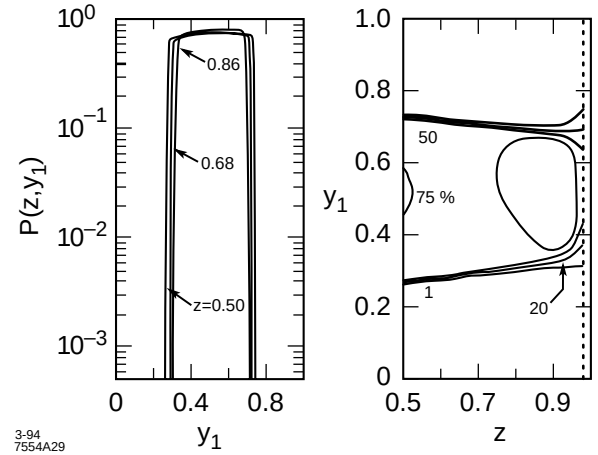

Figure 22. The acceptance $P(z, y_1)$ for semiexclusive production of B mesons at the Z^0 peak. Here $y_1 = y_b$ is the back momentum of the $\bar{b}$ quark in the hadronizing system.

motion. This is an ideal situation, as is reflected in the wide and high plateaus of $P(z, y_1)$ shown in Fig. 22. At large z, when the mass of the hadronizing system is not much larger than m_b, this situation deteriorates rapidly. However, at $z \sim 0.95$ the recoil system still has a mass of more than 20 GeV, so that the endpoint region can be excluded with great accuracy. Thus the rates which we will predict for

semiexclusive B production are extremely insensitive to physics at any scale softer than $\min\{\bar{z}, zy_i\langle\bar{x}\rangle\}m_z^2$.

8. Results

We can now combine the results of the previous sections to obtain predictions for observable cross-sections at realistic energies.

We first perform the convolution of hard-scattering amplitudes and distribution amplitudes; using Eqs. (2.6) and (2.7) and the definitions of Eq. (2.4), we obtain after some rearrangement [3]

$$\begin{aligned}\mathcal{M}^{(+)} = C_F \frac{16\pi^2\alpha\alpha_s}{zQ^2}\Bigg[& 2sce^{-i\phi}\left(q_u\bar{B}\quad\frac{\overline{y_2}}{y_1} - q_sB\quad\frac{\overline{y_1}}{y_2}\right) \\ & + \quad \bar{\bar{z}}s^2e^{-2i\phi}\left(q_sB - q_u\big[\bar{B} + z\bar{A}(z)\big]\frac{y_2}{y_1}\right) \\ & - \quad \bar{\bar{z}}c^2\left(q_u\bar{B} - q_s\big[B + zA(z)\big]\frac{y_1}{y_2}\right)\Bigg]\end{aligned} \tag{8.1}$$

for K^- or longitudinally polarized K^*, and

$$\mathcal{M}^{(+)} = C_F \frac{16\pi^2\alpha\alpha_s}{Q^2}c^2\bar{z}\ \ \frac{q_sA(z)}{y_2} - \frac{q_u\bar{A}(z)}{y_1} \tag{8.2}$$

for transversely polarized K^* mesons. Again, the same result holds for any light flavored meson.

The argument of α_s depends on the diagram; in general, we can use the substitutions

$$q_s\alpha_s \to q_s\alpha_s(\bar{x}zy_2Q^2) \quad \text{and}$$

$$q_u\alpha_s \to q_u\alpha_s(xzy_1Q^2).$$

We will not exhibit the explicit dependence of α_s on the momentum transfer in the equations which follow. However, the final results we present are obtained by

a numerical integration procedure which takes into account the running of α_s for each model wavefunction and for each value of z and y_i.

Squaring the amplitude and summing over polarizations, we obtain the differential cross section

$$\begin{aligned}
\mathrm{d}\sigma = & \frac{4}{9\pi^2}\frac{\alpha^2\alpha_s^2}{Q^4}\frac{\bar{z}}{z}\mathrm{d}z\ \mathrm{d}y_1\ \mathrm{d}\cos\theta\ \mathrm{d}\phi \\
& \times\Bigg\{\frac{\bar{z}}{2}(1+\cos^2\theta) \\
& \qquad \left(\ q_s B - q_u\big(\bar{B}+z\bar{A}(z)\big)\frac{y_2}{y_1}\ ^2 + \ q_u\bar{B} - q_s\big(B+zA(z)\big)\frac{y_1}{y_2}\ ^2\right) \\
& + 2\sin^2\theta\ \ q_s B\quad \overline{\frac{y_1}{y_2}} - q_u\bar{B}\quad \overline{\frac{y_2}{y_1}}\ ^2 \\
& - 4\quad \bar{\bar{z}}\cos\theta\sin\theta\cos\phi \\
& \qquad q_s B\quad \overline{\frac{y_1}{y_2}} - q_u\bar{B}\quad \overline{\frac{y_2}{y_1}}\quad q_s\frac{B+y_1 z A(z)}{y_2} - q_u\frac{\bar{B}+y_2 z\bar{A}(z)}{y_1} \\
& + \bar{z}\sin^2\theta\cos 2\phi\Bigg(\ q_s B\quad \overline{\frac{y_1}{y_2}} - q_u\bar{B}\quad \overline{\frac{y_2}{y_1}}\ ^2 - z^2 q_u q_s A(z)\bar{A}(z) \\
& \qquad + z\ \ q_s B\quad \overline{\frac{y_1}{y_2}} - q_u\bar{B}\quad \overline{\frac{y_2}{y_1}}\quad q_s A(z)\quad \overline{\frac{y_1}{y_2}} - q_u\bar{A}(z)\quad \overline{\frac{y_2}{y_1}}\ \Bigg)\Bigg\}
\end{aligned} \tag{8.3}$$

for helicity-zero, and

$$\mathrm{d}\sigma = \frac{4}{9\pi}\frac{\alpha^2\alpha_s^2}{Q^4}z\bar{z}^2\mathrm{d}z\quad \frac{q_s A(z)}{y_2} - \frac{q_u\bar{A}(z)}{y_1}\ ^2\mathrm{d}y_1\ (1+\cos^2\theta)\mathrm{d}\cos\theta \tag{8.4}$$

for helicity-1 mesons; in the latter case, we have integrated out the trivial ϕ-dependence.

To make use of the portion of the cross section proportional to $(1+\cos^2\theta)$, we must be able to discern it above the direct fragmentation contribution of Eq. (6.4). We must caution the reader that the results of [3] are entirely misleading at this

juncture. The neglect of hadronization in the naive treatment of [3] led to the conclusion that, as $z \to 1$, the endpoints $y \to 0, 1$ would become experimentally accessible. As a result, the $1/y$ behavior of the cross section of Eq. (8.3) was claimed to lead to a substantial signal at large z.

In practice, the reverse holds. As z grows, the small-y growth of the cross section is curtailed not by an experimental cut but through the multiple-scattering process described in Section 5. Meanwhile, the energy in the hadronizing system decreases, so that our ability to isolate the region where y is not small is lost. To prevent unacceptable contamination of the signal, we must impose the harsh cut of Eq. (7.8); as a result, the cross-section for large z is controlled by the $\bar{z}$ factor in Eq. (2.1), and almost no signal can be measured in the region $z > 0.9$.

Numerically, it happens that the signal is actually cleaner at small z. This is because the signal of Eq. (8.3) grows more slowly as $y \to 0$ than the background; thus the ability to reject events with small y is paramount. Since the hadronizing system is more energetic at smaller z, the event shape cuts we use are more effective, and we obtain the best results by integrating over the region $0.5 < z < z_{\max}$. We should choose the upper bound $z_{\max}$ on z to maximize the ratio $S/\sqrt{N}$, where S is the signal of Eq. (8.3) and N the noise from Eq. (6.2) [50]. Examination of the numerical results (using the symmetric wavefunction, so that our cuts will not depend on a model wavefunction) shows that the ratio $S/\sqrt{N}$ is maximized if we use the upper bound $z_{\max} = 0.8$.

To estimate the reliability of our perturbative methods, it is useful to examine the differential cross section $\mathrm{d}\sigma/\mathrm{d}z\mathrm{d}y_1$, as in Fig. 23. For moderate values of z, the hadronizing system is sufficiently energetic to allow excellent rejection of the endpoint region; as z increases, the cross section $\mathrm{d}\sigma/\mathrm{d}z$ comes to be dominated

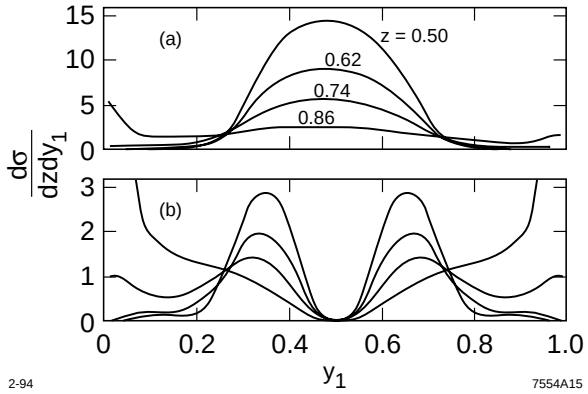

Figure 23. The differential cross section $\mathrm{d}\sigma/\mathrm{d}z\mathrm{d}y_1$ at $\sqrt{s} = 10$ GeV for several values of z, for (a) the ZZC model of the K^- and (b) the asymptotic model of the K^0 (or π^0). As z increases, the cross section comes to be dominated by endpoint contributions, for which perturbative predictions are untrustworthy.

by small momentum transfers $q^2 = zy_{\min}Q^2$. This problem is more severe for neutral mesons with symmetric wavefunctions, as shown in Fig. 23(b), where the amplitude in the central region is suppressed by cancellations between couplings to the two separate quarks. (Naturally, the Dirac form factors of these mesons vanish altogether.)

Table 2 shows the total cross sections expected for semiexclusive production, based on the model wavefunctions of Table 1. What else can we learn from the cross section of Eq. (8.3)? We first consider the term proportional to $\sin^2\theta$:

$$\frac{16}{9\pi}\frac{\alpha^2\alpha_s^2}{Q^4}\frac{\bar{z}}{z}\mathrm{d}z \quad q_s B \quad \frac{\overline{y_1}}{y_2} - q_u\bar{B} \quad \frac{\overline{y_2}}{y_1}^{\,2}\mathrm{d}y_1 \;\; \sin^2\theta\mathrm{d}\cos\theta. \tag{8.5}$$

Since this term depends on the distribution amplitude only through the constant B, it will grow more slowly than $\mathrm{d}\sigma_{\mathrm{sx}}$ at large z. Also, the y-dependence is less pronounced, so that the integral over y_1 will not gain large contributions from terms like y_1^{-2}.

As a result, this contribution to the total cross section is numerically small, amounting to no more than 30% of the total semiexclusive contribution. Since

Table 2

	Distribution	Cross Section σ_{sx} (fb)		
Meson	Amplitude	Charged	Neutral	Ratio
K	ZZC	1.46	0.40	3.6
	Toy	0.55	0.23	2.4
	asymptotic	0.62	0.10	5.9
π	ZZC	1.56	0.88	1.8
	asymptotic	0.36	0.15	2.4
ρ_L	ZZC	0.87	0.20	4.3
ρ_T	ZZC	0.34	0.09	3.9
$K^*{}_L$	ZZC	0.89	0.19	4.8
ϕ	ZZC	0.42	0.09	4.8

the angular distribution of background events is not precisely $1+\cos^2\theta$ due to hadronization effects, a clean separation of this term seems unfeasible.

The existence of an energetic meson introduces a preferred axis into the computation, so that there is no reason to expect the backgrounds to have trivial ϕ-dependence. Since the sign of $\cos\phi$ cannot be determined without successfully tagging the primary quark flavors in the two recoil jets, we are left with only the part of Eq. (8.3) proportional to $\cos 2\phi$, which is numerically much smaller than the dominant $1+\cos^2\theta$ term. Thus isolation of the ϕ-dependent terms in the cross section appears impossible.

From the amplitude of Eq. (2.11), we obtain the unpolarized differential cross section for semiexclusive production of 0^+ mesons:

$$\mathrm{d}\sigma = \frac{\pi\alpha^2\alpha_s^2 q_i^2}{24Q^4}\ \frac{\bar{z}}{z}\mathrm{d}z\ \mathrm{d}y_1\ \mathrm{d}\cos\theta\ \mathrm{d}\phi \left\{ \frac{4}{y_1 y_2}\ 2\bar{z}B_{gg} + \frac{z f_{gg}}{2\ \overline{3}}^{\ 2} \sin^2\theta \right.$$
$$\left. + \bar{z}\left(\frac{1}{y_1^2} + \frac{1}{y_2^2}\right)\ (2-z)B_{gg} + \frac{f_{gg}}{2\ \overline{3}}^{\ 2}(1+\cos^2\theta)\right\},$$

where we have integrated over $\mathrm{d}\phi$. Here q_i^2 is the QED coupling of the recoil quark, which should be summed over all quark flavors. However, we should not make the substitution 3 $q_i^2 \to R_{e^+e^-}(\bar{z}Q^2)$, since production of a gg state recoiling against a resonance is suppressed by final-state interactions (see Section 2.5). Instead, we consider only the light quarks u, d, and s; our events shape cuts will strongly suppress the signal from events like $e^+e^- \to f_0 c\bar{c}$, where the thrust of the recoil system is unlikely to be large.

The gluons are produced collinearly, and are nominally on shell (up to corrections of order the meson mass). We use the fixed coupling $\alpha_s = 0.4$, reflecting our belief that the small size of the meson will limit the growth of the running coupling.

To estimate the semiexclusive cross section, we first use the asymptotic wavefunction $\phi_{gg}(x) = \overline{3} f_{gg} x\bar{x}$. Then $B_{gg} = f_{gg}\ \overline{3}/2$, and the semiexclusive cross section scales as f_{gg}^2. With the cuts of Eqs. (7.7) and (7.8), we obtain an observed integrated cross section of $71 f_{gg}^2$ fb GeV^{-2}.

Figure 24 shows the resulting differential cross section $\mathrm{d}\sigma/\mathrm{d}z$. It falls off rapidly with increasing z, reflecting the fact that glueball production is forbidden

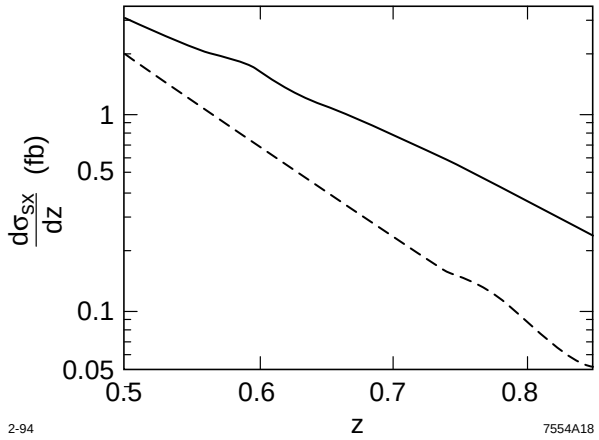

Figure 24. The differential cross section $\mathrm{d}\sigma/\mathrm{d}z$ for semiexclusive production of gg states at the Υ_{4s} with $J_z = 0$ (solid line) and $J_z = 2$ (dashed line). We have used the *ansatz* that the gluon distribution is proportional to $x\bar{x}$, normalized to $f_{\mathrm{gg}} = 100$ MeV. The latter is probably somewhat optimistic.

at leading twist in the exclusive limit. The behavior of $\mathrm{d}\sigma/\mathrm{d}z$ is well approximated by $\exp(-7z)$ for scalar or longitudinally polarized states and by $\exp(-10.5z)$ for transversely polarized states.

The angular distribution arising from our *ansatz* for the two-gluon distribution amplitude is also noteworthy. The observed distrbution, after implementation of our acceptance cuts, is very closely approximated by

$$\frac{\mathrm{d}\sigma_{\mathrm{sx}}}{\mathrm{d}\cos\theta} \propto 1 - 0.19\cos^2\theta$$

over the entire region $0.5 < z < 0.8$. This seems to be a numerical peculiarity of the asymptotic distribution amplitude; using instead the 'double-humped' distribution amplitude

$$\phi(x) \propto x\bar{x}(x-\bar{x})^2$$

predicts an angular distribution which varies from $1 - 0.20\cos^2\theta$ at $z = 0.5$ to $1 - 0.08\cos^2\theta$ at $z = 0.8$, as well as increasing the total cross section to 160 f_{gg}^2 fb GeV^{-2}.

Note that f_{gg} will not be larger than about 100 MeV, so these cross sections are commensurate with our predictions for $q\bar{q}$ mesons. However, they have the advantage of being peaked at smaller values of z, where the hadronizing system is more energetic and pQCD predictions less subject to soft corrections. The primary theoretical drawback is the α_s^2 dependence of the cross section, which introduces substantial uncertainty into the predicted normalization of the semiexclusive cross section.

We can similarly compute the total cross section for production of 2^+ mesons. With the additional assumption that $\phi_{gg/L} = \phi_{gg/T}$, we obtain after all experimental cuts the result $\mathrm{d}\sigma_{\mathrm{sx}} = 103 f_{gg}^2 \mathrm{fb}/\ \mathrm{GeV}^{-2}$, again using the asymptotic form of the distribution.

8.2 Direct photon production

Using the kinematics of Section 2, we can easily compute the amplitude for direct-photon production. The result is

$$\mathcal{M}^{(++)} = \frac{C_F e^3 q_e q_i}{z} \left(c \quad \overline{y_2} + s e^{i\phi} \quad \overline{\bar{z} y_1} \right)^2 \quad \frac{q_i}{\overline{y_1 y_2}} + \frac{q_e}{\overline{\bar{z}} s c e^{i\phi}}$$

when the photon, electron, and antiquark share the same helicity; the results for other helicities are obtained by $s \leftrightarrow c$ and $y_1 \leftrightarrow y_2$. In this case the color factor $C_F = \quad \overline{3}$.

The direct photon production cross section is much less well behaved at the endpoints, since the mechanisms described in Section 6 do not affect its collinear divergences. Thus our methods do not suffice to accurately estimate the cross section for direct photon production in these regions. To gain some feel for the

comparative size of these cross sections, however, we may consider the ratio of amplitudes away from the collinear region.

We must consider the possibility that γ-K^0 or γ-π^0 misidentification could represent a substantial background to the semiexclusive signal. We find that at $\overline{s} = 10$ GeV, direct photon cross sections are typically 20–50 times the semiexclusive cross sections in which we are interested, so that γ rejection must be complete to less than 1% in order to allow clean extraction of the semiexclusive signal. At these energies, semiexclusive events do not constitute a significant background to direct photon production; however, at lower energies where the Q^{-2} suppression is less drastic, they must be considered.

8.3 Z^0 DECAYS

The program implemented to search for semiexclusive events in Z decays is similar to that above. The experimental cut changes in appearance but not in substance, as described in Section 7.3.

The simple substitutions $q_i \to \mathbf{Q}_i$, $e \to g$, and $Q^4 \to m_Z^2, {}^2_Z$ enable us to compute the cross sections at the Z peak without further ado. In this case, the wide acceptance allowed by Eq. (7.9)means that the predictions of Ref. [3] were overly pessimistic. On the other hand, the considerations of Section 2.3 show that the D and B wavefunctions probed at $Q = m_Z$ will not be very strongly peaked, so that the hard-scattering amplitudes themselves will not see the wavefunction enhancement described in Ref. [3]. For light mesons, the consequences of evolution are even more pronounced, and it will be impossible to extract information about the distribution amplitude at such high energies.

Table 3

	Distribution	Branching Ratio , sx ($\times 10^{-6}$)		
Meson	Amplitude	Charged	Neutral	Ratio
K	ZZC	1.53	0.76	2.0
	Toy	0.98	0.49	2.0
	asymptotic	0.91	0.41	2.2
π	ZZC	1.16	0.32	3.7
	asymptotic	0.56	0.14	4.1
ρ_L	ZZC	0.70	0.18	3.9
ρ_T	ZZC	0.44	0.11	4.0
$K^*{}_L$	ZZC	1.00	0.46	2.2
ϕ	ZZC	1.26	0.39	3.2

We again follow the same program of computing the acceptance, then integrating the cross section over $\mathrm{d}y_1\mathrm{d}z$ to obtain observable quantities. The acceptance is shown in Fig. 20 and the resulting cross sections in Table 3.

8.4 Heavy-quark mesons

The analysis of semiexlusive reactions is particularly rewarding in the study of heavy-quark mesons. This is largely due to the sensitivity of the production cross section to the extent to which the distribution amplitude is peaked at large momentum fraction x, which is closely related to the moment $\langle x \rangle$ of the distribution amplitude. These moments have been the subject of substantial theoretical interest [51,52], but precise experimental determinations have so far been unavailable.

We wish to extract a relation between the moment $\langle x \rangle$ and the integrated semiexclusive production cross section σ_{sx}. Both of these quantities depend on

some complicated distribution amplitude, which will introduce model-dependence into the relationship. We estimate this dependence by using three simple models for the distribution amplitudes of heavy-light mesons.

The first is the toy model of Ref. [3],

$$\phi(x) = f_h \quad \overline{3}\frac{(1-x)(x-x_0)}{(1-x_0)^3} \qquad \text{with} \quad x_0 = 2\langle x\rangle - 1.$$

Because this distribution is symmetric about $\langle x\rangle$ and has no small-x 'tail,' it is less concentrated at very large x than we would expect for a realistic wavefunction, and will thus lead to somewhat lower estimates of $\sigma_{\rm sx}$.

The second model is simply

$$\phi(x) = \frac{(n+1)(n+2)}{2 \quad \overline{3}} f_h x^n \bar{x} \qquad \text{with} \quad n = \frac{2}{\langle 1-x\rangle} - 3.$$

This yields a distribution which is very strongly peaked at x near 1, and which thus provides an estimate of of $\sigma_{\rm sx}$ for given $\langle x\rangle$ which may be unrealistically large. However, it is more realistic than the toy distribution from Ref. [3] used above.

The final model wavefunction is derived from the wavefunction given in Ref. [51], which is chosen to maximize $\langle x\rangle$ subject to the constraints of unitarity and of the values of the decay constant and quark and meson masses. Integrating the wavefunction described in Ref. [51] over all $k_\perp$, we obtain the distribution amplitude

$$\phi(x) = \frac{3 \quad \overline{3}}{2} f_h (1-x) \;\; x(1+2x_0)\ln\Big(\frac{1+2x}{1+2x_0}\Big) - 2x_0(x-x_0) \tag{8.6}$$

with

$$\begin{aligned}\langle x\rangle &= \frac{81}{64}\frac{1+2x_0}{(1-x_0)^4}\ln\Big(\frac{3}{1+2x_0}\Big) - \frac{(2+x_0)(13+40x_0-38x_0^2+12x_0^3)}{32(1-x_0)^3} \\ &\simeq \frac{3+2x_0}{5} - 0.0138(1-x_0)^2 + \cdots\end{aligned}$$

Under the assumption that the wavefunction $\psi_{D\to c\bar{q}}$ is purely real and positive, the methods of Ref. [51] can be used to obtain the upper bound $\langle x\rangle < 0.72$, in contrast to the estimate $\langle x\rangle = 0.79$ of Ref. [15]. The unitarity-saturating wavefunction of Eq. (8.6) is more strongly peaked toward $x = 1$ than the toy model, and is still extremely asymmetric; thus it should not substantially underestimate the rate of semiexclusive production when compared to realistic models. The three model distribution amplitudes are shown in Fig. 25 for $\langle x\rangle = 0.72$ and 0.84, which are the unitarity bounds of Ref. [51] for the D and B mesons respectively.

With the acceptance functions described in Section 7.4, it is now a simple matter to compute the cross sections for semiexclusive production at the Υ_{4s} resonance. The dependence of the total cross section on $\langle x\rangle$ is displayed in Fig. 26. The error bars shown do *not* represent data, but serve to indicate the degree of model dependence in the prediction. The uncertainty in $\langle x\rangle$ due to model dependence is on the order of 0.03, which is roughly equal to the uncertainty introduced by a 60% error in the measurement of $\sigma_{\rm sx}$. Since both the charged and neutral channels can be used in this measurement, the model dependence will probably be the dominant source of error. If constraints on the limiting behavior of $\phi(x)$ as $x \to 1$ can be obtained independently, they would serve to eliminate the source of most of this model dependence.

At the Z^0 peak, the prospects for probing D meson structure are exceedingly dim, largely due to the erosion of nonperturbative wavefunction information during the evolution to the large momentum scales in question. However, there is now sufficient energy to produce B mesons in perturbative processes, and we can ask the same questions about their distribution.

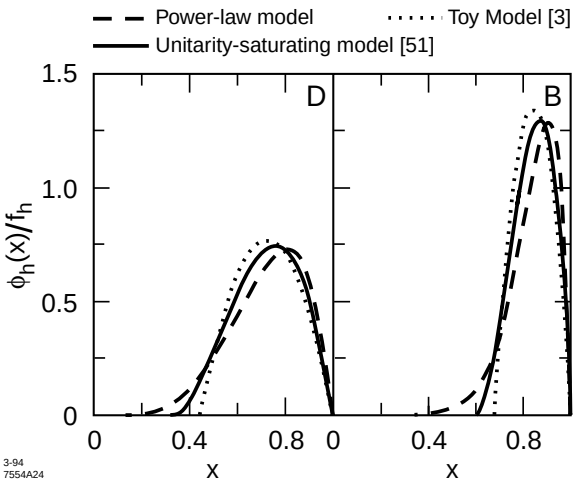

Figure 25. Three models of the distribution amplitudes of the B and D mesons, parametrized to yield $\langle x_c \rangle = 0.72$ and $\langle x_b \rangle = 0.84$. We assume $f_B = f_D = 190$ MeV.

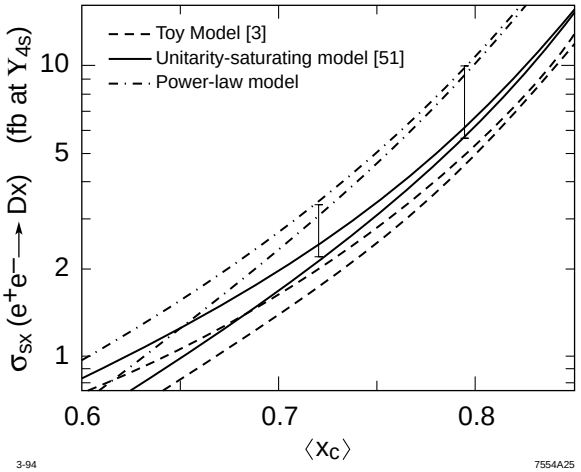

Figure 26. The semiexclusive D production cross section at Υ_{4s} energies as a function of $\langle x \rangle$, for the three models shown in Fig. 25. The error bars shown serve to indicate the extent of model dependence. The upper curves describe charged D production; the lower, neutral.

The apparent conflict between QCD sum rules [15,53], which provide the estimate $\langle x \rangle = 0.90$, and unitarity constraints which suggest $\langle x \rangle < 0.84$, exists in this case as well. Though both of the above arguments are predicated on small momentum transfer, it is still of interest to measure the moment $\langle x_b \rangle$ in

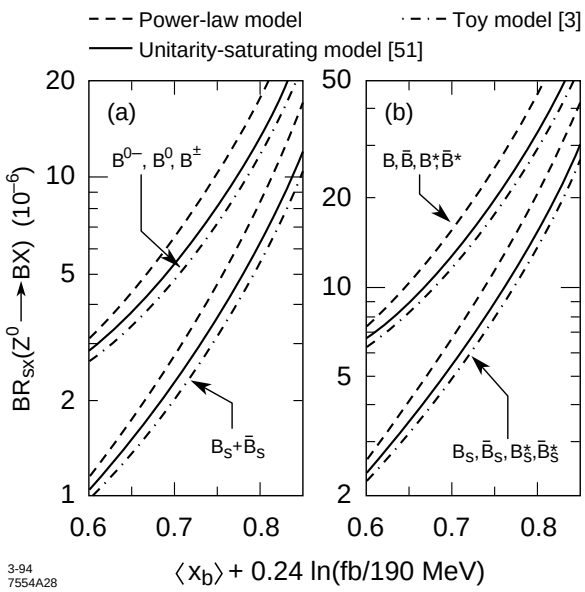

Figure 27. Semiexclusive branching ratios for B mesons produced in Z decay. In (a), the upper curve sums contributions from B^0, $\bar{B}^0$, B^+, and B^- mesons while the lower curve gives the branching fraction to B_s and $\bar{B}_s$ mesons. The parameter $\langle x \rangle$ need not be the same in the two cases. In (b), we have included the contributions from the first excited states B^*, summed over polarizations, so that $\langle x \rangle$ is not precisely defined.

semiexclusive production at the Z, though one must bear in mind the remarks of Section 2.3.

The expected cross sections for semiexclusive B production at the Z are shown in Fig. 27. Again, the model dependence is substantial, leading to an uncertainty of about 0.03 in the extraction of $\langle x \rangle$. However, the branching fractions are sufficiently large that at least an approximate measurement may be possible in the current LEP experiments [54]. This measurement will provide crude but essential information about the structure of the B meson.

Figure 28 shows the dependence on $\langle x \rangle$ of the ratio of semiexclusive neutral to charged B production. Although this is a very difficult measurement from an experimental standpoint, its relative model-independence is striking.

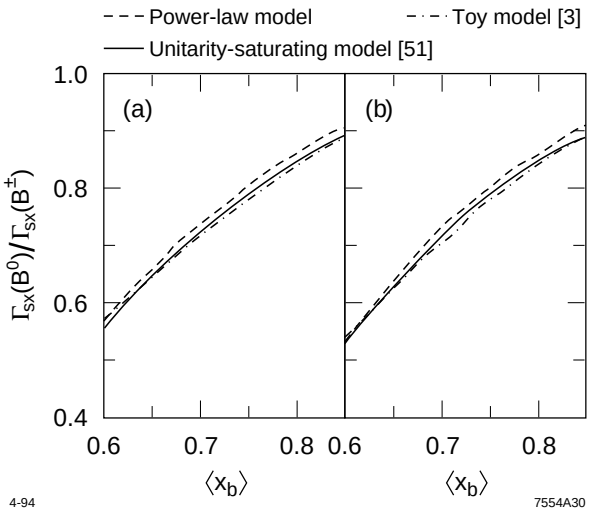

Figure 28. The ratio of neutral to charged B production as a function of $\langle x \rangle$. In (a), only the pseudoscalar B states are considered; in (b), we sum contributions from B and B^* production.

In examining Figs. 27 and 28, one must bear in mind that the moment $\langle x \rangle$ being measured does not correspond directly to that computed in Refs. [15,51,53] due to the effects of evolution. Also, the total cross sections shown in Fig. 27 are proportional to f_B^2, which is itself subject to substantial uncertainty.

Note that the abcissa of Fig. 27 is $\langle x \rangle + 0.24 \ln(f_B/190 \text{ MeV})$, to compensate for the f_B-dependence of the cross section. Since the cross section does not rise precisely exponentially with $\langle x \rangle$, this introduces some imprecision; however, the resulting errors are negligible. Over the region of phenomenological interest, $150 < f_B < 250$ MeV and $0.6 < \langle x \rangle < 0.8$, they introduce an error of less than 0.005 into the measurement of $\langle x \rangle$.

The average momentum fraction $\langle z \rangle$ is very mildly dependent on $\langle x \rangle$: $\mathrm{d}\langle z \rangle / \mathrm{d}\langle x \rangle \simeq 0.1$. Since it is unrealistic to expect that enough events can be gathered to evaluate $\langle z \rangle$ with any precision, this does not provide us with an independent determination of $\langle x \rangle$.

8.5 Extraction of moments of the distribution amplitude

To test the validity of the approach of Ref. [13], in which the moments $(x-\bar{x})^n\phi(x)\mathrm{d}x$ of the distribution amplitude ϕ are extracted from QCD sum rules, we wish to obtain the same quantities directly from experiment. As we have shown, the experimentally observable quantities are entirely determined by the integrals $A, \bar{A}, C$, and $\bar{C}$ of Eq. (2.4). Thus, to reconstruct the moments from experiment without recourse to model calculations, we must be able to fit the integrand $(x-\bar{x})^n$ which enters into the computation of moments to a sum of the integrands

$$\frac{1}{\bar{x}(1-zx)} \qquad \text{and} \qquad \frac{1}{x(1-z\bar{x})}$$

which determine $A(z)$ and $\bar{A}(z)$.

Figure 29(a) shows the results of such an attempt. Here we have assumed that $A(z)$ and $\bar{A}(z)$ may be measured in eight bins evenly spaced from $z = 0.5$ to $z = 1$, and that B and $\bar{B}$ are known. We used MINUIT to minimize the difference of the moment and fit integrands under the $\mathcal{L}^2$ metric with weight $x\bar{x}$ [55]. Figure 29(a) shows the moment integrands and the best fits to them: for example, when attempting to reconstruct the 0^{th} moment (the decay constant) from the measured values of A and $\bar{A}$, we end up integrating not $\phi(x)$, but $\phi(x)$ multiplied by the function shown as a solid line in Fig. 29(a). One could say that the line represents the best available approximation to 1.

For $n = 0$ or 1, the fit is tolerably good. However, the fit for $n = 2$ is unacceptable; this situation persists even if we increase the number of bins to 20 (Fig. 29(b)). Thus we are forced to conclude that only the first moment can be measured model-independently with any accuracy in semiexclusive processes.

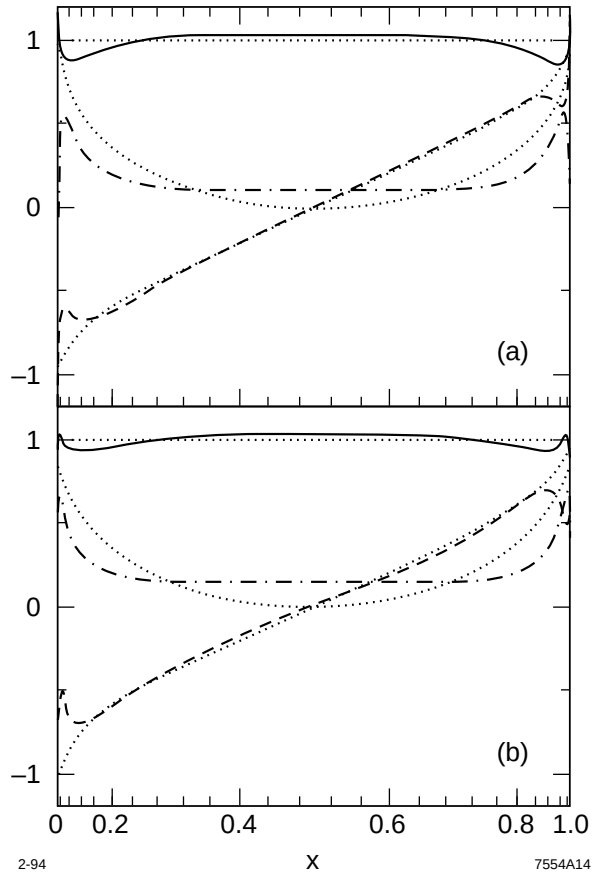

Figure 29. Reconstruction of the integrands $(x - \bar{x})^n$, required for calculation of moments of the distribution amplitude, from the integrands in the transforms $A(z)$ and $\bar{A}(z)$. The fitted curves sum contributions from $A(z)$ and $\bar{A}(z)$ at (a) eight points; (b) 20 points. Note that the scale of x is distorted to show the metric of integration.

8.6 Conclusions

We have analyzed semiexclusive meson production in some detail, noting the obstacles to unambiguous theoretical calculations and to clean experimental results. The most difficult remaining obstacle is the poorly understood behavior of the recoil system during hadronization, which will make it difficult to accurately predict the rate of background events for a given choice of experimental cuts.

Some progress can be made by appealing to the expectation [22] that the soft backgrounds should scale as $\exp\{-2\Delta Y\}$, or equivalently as $\exp\{2Y_{\max}\}$.

Since the semiexclusive events we wish to observe are intrinsically hard, the cross section $\mathrm{d}\sigma_{\mathrm{sx}}/\mathrm{d}Y_{\mathrm{max}}$ should decrease less rapidly with decreasing Y_{max} than the soft background rate; thus it should be possible to fit separate curves to the background and signal rates. At the values of Y_{max} proposed here, we find that the behavior of the semiexclusive signal is well approximated by $\exp\{1.6\ Y_{\mathrm{max}}\}$.

The intrinsic hardness of any process producing a strongly isolated meson is a double-edged sword. On the one hand, it places us in a region in which Monte Carlo predictions of the expected background are extremely unreliable; however, it also tells us that the scattering producing the meson is dominated by short-distance physics. Thus we have good reason to believe that the mechanism we have considered will account for the bulk of the observed cross section. We have obtained several wavefunction-independent predictions, such as the Y_{max} dependence of the observed signal, which can be used to test the consistency of this view.

Figure 30 shows the differential semiexclusive production cross section for K mesons as a function of z, for our three models of the kaon distribution amplitude. Besides the absolute normalization, which indicates the extent to which the distribution is concentrated near the endpoints, there are two noteworthy features of Fig. 30.

First, the ratio between charged and neutral production cross sections is a sensitive test of the asymmetry ϕ_K. A symmetric distribution leads to efficient cancellation between the q_s- and q_d-dependent parts of the amplitude for K^0 production, and hence to a very large predominance of charged kaons. The extremely asymmetric toy distribution yields a comparatively small ratio. This ratio is largely immune to effects from our treatment of soft physics, and provides

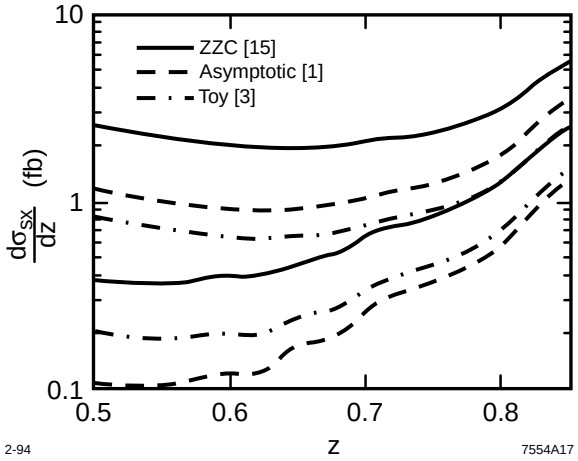

Figure 30. The differential cross section $d\sigma_{sx}/dz$ for semiexclusive K production, for three models of ϕ_K. In each case, the upper line shows the rate for K^-, the lower for K^0. The unevenness in the lines arises from statistical fluctuations in our Monte Carlo calculations of the acceptance $P(z, y_1)$ near the endpoints. It is more pronounced for neutral than for charged production; see Fig. 23.

a sensitive test of models for ϕ_K. Predictions from each model distribution are included in Table 2.

Second, contrary to the conclusions of Ref. [3], we find that the shape of the cross section depends only weakly on the distribution amplitude chosen. Thus comparison with the observed differential cross section will serve more to test the validity of our picture of semiexclusive production than to place constraints on models of the hadron. If we define the expectation value $\langle z \rangle_{0.5}^{0.8}$ of z for all mesons with $0.5 < z < 0.8$, we obtain $\langle z \rangle_{0.5}^{0.8} = 0.66 - 0.67$ for all three distributions under consideration.

Finally, we have noted that the rate of semiexclusive production provides a sensitive measurement of the first moment $\langle x \rangle$ of the distribution amplitudes of heavy-light mesons. This will provide welcome experimental input to a field where comparisons between theory and experiment are often elusive.

We conclude that at integrated luminosities between 10 and 100 fb^{-1}, the analysis of semiexclusive production has limited but significant applicability to the study of mesonic structure. If still larger event samples can be obtained, several new avenues of exploration will open within the same framework. Most of these have been touched upon here. For example, discrimination between the asymptotic and ZZC models of ϕ_K through a precise measurement of $\langle z \rangle_{0.5}^{0.8}$ would require a clean sample of a few hundred semiexclusive events, as would a model-independent reconstruction of the first moment of the distribution amplitude or a precise measurement of the angular dependence of $\mathrm{d}\sigma/\mathrm{d}\omega$.

ACKNOWLEDGEMENTS

We thank S. Brodsky, G. Sterman, A. Mueller, J. Bjorken, H. Lu, P. Burrows, A. Lath, A. Weidemann, G. Bonvicini, and M. Peskin for helpful conversations. This work was supported by Department of Energy contract DE-AC03-76SF00515.

APPENDIX A: Computation of Hard-scattering Amplitudes

Section 2 defines our frame of reference; for definiteness, we will let l_1 and l_2 refer to the momenta of the outgoing quark and antiquark of the recoil system, respectively.

The method of Ref. [11] takes advantage of the fact that in the chiral representation of the Dirac algebra, each of the matrices γ^μ has block-diagonal entries of zero. Thus we can work with effective two-component matrices $\gamma_+^\mu = (1, \vec{\sigma})^\mu$ and $\gamma_-^\mu = (1, -\vec{\sigma})^\mu$, and corresponding two-element spinors satisfying $\not{p}_\pm u_\mp(p) = 0$ and $u_\pm(p) u_{\ \pm}(p) = \not{p}_\pm(p)$.

Spinor amplitudes are constructed like ordinary four-component amplitudes, with the simplifying rules $\gamma^\mu_\pm \gamma^\nu_\pm \equiv 0$ and $\gamma^\mu_\pm u_\pm(p) \equiv 0$ serving to enforce helicity conservation along fermion lines. Since $u_+(p)$ is the correct spinor for a fermion with positive helicity, or an antifermion with negative helicity, this method serves admirably for the construction of individual helicity amplitudes.

The algebra is greatly simplified by the Fierz relation

$$g_{\mu\nu}(\gamma^\mu_\pm)^i_j(\gamma^\nu_\mp)^k_l = \delta^i_l\delta^k_j,$$

so that all internal Lorentz indices may be effortlessly contracted. Subscripts may be flipped by use of the relation

$$u_{\ \pm}(p)\gamma^\mu_\mp \cdots u_\pm(q) = \tilde{u}_{\ \pm}(q)\cdots\gamma^\mu_\pm \tilde{u}_\pm(p),$$

where $\tilde{u}_\mp \equiv i\sigma^2 u^*_\pm$. It is convenient, though not necessary, to define spinors to satisfy the additional relationship $\tilde{u}_\pm = \pm u_\pm$.

As in Section 2, we define $E \equiv E_{\rm beam}$, $s \equiv \sin(\theta/2)$, and $c \equiv \cos(\theta/2)$. With these definitions, the explicit momenta are:

$$\begin{aligned}
k &= E(1, 2sc\cos\phi, 2sc\sin\phi, c^2 - s^2) && \text{for the incoming electron or photon;}\\
k' &= E(1, -2sc\cos\phi, -2sc\sin\phi, s^2 - c^2) && \text{for the incoming positron or photon;}\\
p &= E(z, 0, 0, z) && \text{for the directly produced meson;}\\
l_1 &= E(y_1 + \bar{z}y_2, 2\sqrt{\bar{z}y_1y_2}, 0, \bar{z}y_2 - y_1) && \text{for the outgoing quark; and}\\
l_2 &= E(y_2 + \bar{z}y_1, -2\sqrt{\bar{z}y_1y_2}, 0, \bar{z}y_1 - y_2) && \text{for the outgoing antiquark.}
\end{aligned}$$

The corresponding matrices and spinors are:

$$
\begin{aligned}
\not{k}_+ &= 2E \begin{pmatrix} c^2 & sce^{-i\phi} \\ sce^{i\phi} & s^2 \end{pmatrix}, & u_+(k) &= \overline{2E} \begin{pmatrix} c \\ se^{i\phi} \end{pmatrix}; \\
\not{k}_- &= 2E \begin{pmatrix} s^2 & -sce^{-i\phi} \\ -sce^{i\phi} & c^2 \end{pmatrix}, & u_-(k) &= \overline{2E} \begin{pmatrix} -se^{i\phi} \\ c \end{pmatrix}; \\
\not{k}'_+ &= 2E \begin{pmatrix} s^2 & -sce^{-i\phi} \\ -sce^{i\phi} & c^2 \end{pmatrix}, & u_+(k') &= \overline{2E} \begin{pmatrix} se^{-i\phi} \\ -c \end{pmatrix}; \\
\not{k}'_- &= 2E \begin{pmatrix} s^2 & sce^{-i\phi} \\ sce^{i\phi} & s^2 \end{pmatrix}, & u_-(k') &= \overline{2E} \begin{pmatrix} c \\ se^{-i\phi} \end{pmatrix}; \\
\not{p}_+ &= 2E \begin{pmatrix} z & 0 \\ 0 & 0 \end{pmatrix}, & u_+(p) &= \overline{2E} \begin{pmatrix} \overline{z} \\ 0 \end{pmatrix}; \\
\not{p}_- &= 2E \begin{pmatrix} 0 & 0 \\ 0 & z \end{pmatrix}, & u_-(p) &= \overline{2E} \begin{pmatrix} 0 \\ \overline{z} \end{pmatrix}; \\
\not{l}_{1+} &= 2E \begin{pmatrix} \bar{z}y_2 & \overline{\bar{z}y_1y_2} \\ \overline{\bar{z}y_1y_2} & y_1 \end{pmatrix}, & u_+(l_1) &= \overline{2E} \begin{pmatrix} \overline{\bar{z}y_2} \\ \overline{y_1} \end{pmatrix}; \\
\not{l}_{1-} &= 2E \begin{pmatrix} y_1 & -\overline{\bar{z}y_1y_2} \\ -\overline{\bar{z}y_1y_2} & \bar{z}y_2 \end{pmatrix}, & u_-(l_1) &= \overline{2E} \begin{pmatrix} -\overline{y_1} \\ \overline{\bar{z}y_2} \end{pmatrix}; \\
\not{l}_{2+} &= 2E \begin{pmatrix} \bar{z}y_1 & -\overline{\bar{z}y_1y_2} \\ -\overline{\bar{z}y_1y_2} & y_2 \end{pmatrix}, & u_+(l_2) &= \overline{2E} \begin{pmatrix} \overline{\bar{z}y_1} \\ -\overline{y_1} \end{pmatrix}; \\
\not{l}_{2-} &= 2E \begin{pmatrix} y_2 & \overline{\bar{z}y_1y_2} \\ \overline{\bar{z}y_1y_2} & \bar{z}y_1 \end{pmatrix}, & u_-(l_2) &= \overline{2E} \begin{pmatrix} \overline{y_2} \\ \overline{\bar{z}y_1} \end{pmatrix}.
\end{aligned}
$$

One useful fact is that amplitudes for negative-helicity electrons, which contain a factor $u_-(k')\gamma_+^\mu u_-(k) = \tilde{u}_+(k)\gamma_-^\mu \tilde{u}_+(k')$, can be changed into their positive-helicity counterparts by the substitutions $se^{-i\phi} \to c$ and $c \to se^{i\phi}$. Alternatively, we can multiply the amplitudes with positive e^- helicity by a phase factor $e^{-2i\phi}$, so that the positive-helicity amplitudes are obtained from their negative-helicity counterparts by the substitution $c \leftrightarrow s$.

The hard-scattering amplitudes for the e^+e^- annihilation processes considered in this paper are given in the text for positive-helicity electrons; we do not present the results for negative-helicity electrons, which can be derived trivially by applying the above observation.

APPENDIX B: Photon-photon collisions

For the calculation of two-photon amplitudes, we must also find a representation of the polarization vectors. This is most easily accomplished in axial gauge with reference vector parallel to p^μ, so that

$$\not{\epsilon}(k,\uparrow) = \frac{|k_+\rangle\langle p_+| + |p_-\rangle\langle k_-|}{\langle k_-|p_+\rangle}, \quad \text{and}$$
$$\not{\epsilon}(k,\downarrow) = \frac{|p_+\rangle\langle k_+| + |k_-\rangle\langle p_-|}{\langle p_-|k_+\rangle}.$$

The amplitudes for these processes are generally quite complicated. However, for $\gamma_\uparrow\gamma_\uparrow \to K^-\bar{s}_- u_+$, the amplitude factors to

$$T_H = \frac{1}{sc}\frac{z}{x} \quad \frac{\overline{y_1}}{y_2}\left[\frac{q_s \quad \overline{y_1}}{\bar{u}_-(l_1)u_+(k)} - \frac{q_u \quad \overline{y_2}}{\bar{u}_-(l_2)u_+(k)}\right]\left[\frac{q_s \quad \overline{y_1}}{\bar{u}_-(l_1)u_+(k')} - \frac{q_u \quad \overline{y_2}}{\bar{u}_-(l_2)u_+(k')}\right]; \tag{B.1}$$

the amplitude for $\gamma_\downarrow\gamma_\downarrow$ is obtained by the replacements $x \to \bar{x}$, $T_H \to T_H^*$, $y_1 \leftrightarrow y_2$.

We are unable to obtain such a simplification for the case in which the photons have opposite helicity. The hard-scattering amplitude for semiexclusive K production from a $\gamma_\uparrow\gamma_\downarrow$ initial state is

$$
\begin{aligned}
T_H = \frac{q_s^2}{zy_2}\Bigg[& \frac{se^{-i\phi}z \quad \overline{y_1}\big((1-zx)c \quad \overline{y_2}+se^{-i\phi} \quad \overline{\bar{z}y_1}\big)}{x\bar{x}(1-zx)} \\
& + \frac{z(c \quad \overline{\bar{z}y_2}+se^{-i\phi} \quad \overline{y_1})(c^2-y_1)}{x(c \quad \overline{\bar{z}y_2}+se^{i\phi} \quad \overline{y_1})} - \frac{z \quad \overline{y_1y_2}(c \quad \overline{\bar{z}y_2}+se^{-i\phi} \quad \overline{y_1})}{\bar{x}(c \quad \overline{y_2}-se^{-i\phi} \quad \overline{\bar{z}y_1})}\Bigg] \\
& + \frac{zq_uq_s(y_2-s^2)^2}{\big(z\bar{x}(y_2-s^2)-|c \quad \overline{y_2}-se^{i\phi} \quad \overline{\bar{z}y_1}|^2\big)(c \quad \overline{\bar{z}y_2}+se^{i\phi} \quad \overline{y_1})(c \quad \overline{y_2}+se^{i\phi} \quad \overline{\bar{z}y_1})} \\
& + \frac{q_uq_s}{zx(y_1-s^2)-|c \quad \overline{y_1}-se^{i\phi} \quad \overline{\bar{z}y_2}|^2}\Bigg[\frac{z^2y_1y_2}{(c \quad \overline{\bar{z}y_1}-se^{i\phi} \quad \overline{y_2})(c \quad \overline{y_1}-se^{i\phi} \quad \overline{\bar{z}y_2})} \\
& + \frac{z \quad \overline{y_1y_2}(c \quad \overline{\bar{z}y_2}+se^{-i\phi} \quad \overline{y_1})}{\bar{x}(c \quad \overline{y_1}-se^{i\phi} \quad \overline{\bar{z}y_2})} - \frac{z \quad \overline{y_1y_2}(c \quad \overline{y_2}+se^{-i\phi} \quad \overline{\bar{z}y_1})}{x(c \quad \overline{\bar{z}y_1}-se^{i\phi} \quad \overline{y_2})} \\
& - \frac{(c \quad \overline{y_2}+se^{-i\phi} \quad \overline{\bar{z}y_1})(c \quad \overline{\bar{z}y_2}+se^{-i\phi} \quad \overline{y_1})}{x\bar{x}}\Bigg] \\
& + \frac{q_u^2}{zy_1}\Bigg[\frac{cz \quad \overline{y_2}\big(c \quad \overline{\bar{z}y_2}+(1-z\bar{x})se^{-i\phi} \quad \overline{y_1}\big)}{x\bar{x}(1-z\bar{x})} \\
& + \frac{z(c \quad \overline{\bar{z}y_2}+se^{-i\phi} \quad \overline{y_1})(s^2-y_2)}{\bar{x}(c \quad \overline{y_2}+se^{i\phi} \quad \overline{\bar{z}y_1})} - \frac{z \quad \overline{y_1y_2}c \quad \overline{y_2}+se^{-i\phi} \quad \overline{\bar{z}y_1})}{xc \quad \overline{\bar{z}y_1}-se^{i\phi} \quad \overline{y_2})}\Bigg].
\end{aligned}
$$

We also consider the semiexclusive production of vector mesons. The amplitude for $\gamma_\uparrow\gamma_\uparrow \to K^*_\uparrow \bar{s}_- u_-$ is

$$
T_H = \frac{1}{sc}\frac{\bar{z} \quad \overline{y_1y_2}}{x\bar{x}}\left[\frac{q_s \quad \overline{y_1}}{\bar{u}_-(l_1)u_+(k)} - \frac{q_u \quad \overline{y_2}}{\bar{u}_-(l_2)u_+(k)}\right]\left[\frac{q_s \quad \overline{y_1}}{\bar{u}_-(l_1)u_+(k')} - \frac{q_u \quad \overline{y_2}}{\bar{u}_-(l_2)u_+(k')}\right].
$$

The corresponding amplitude for $\gamma_\downarrow\gamma_\downarrow$ vanishes.

Again, we are unable to find a simple form for the case of opposite photon helicities. The semiexclusive hard-scattering amplitude for $\gamma_\uparrow\gamma_\downarrow \to K^*_\uparrow \bar{s}_- u_-$ is extremely awkward, and to present it here would serve no purpose.

In the same-helicity case, however, note that the x-dependence of T_H is subsumed into an overall constant [56]; the interplay between the internal momentum fraction x and the kinematic observables y_i and z, which is the

major motivation for studying semiexclusive processes, is absent. As a result, the semiexclusive cross section is no more valuable than the form factor in studying the meson wavefunction; we can predict only an absolute normalization, which experience teaches us is the least reliable and least valuable type of prediction. Since the normalization also suffers from additional uncertainties arising from the case $\vec{l}_i \parallel \vec{k}$, where pQCD is less important than vector-meson dominance, we must conclude that two-photon semiexclusive processes promise no insight into the structure of hadrons.

REFERENCES

[1] G.P. Lepage and S.J. Brodsky, *Phys. Rev.* **D22**, 2157 (1980).

[2] V.N. Baier and A.G. Grozin, *Phys. Lett.* **96B**, 181 (1980); A.G. Grozin. *Sov. J. Nucl. Phys.* **37**, 255 (1983); V.N. Baier and A.G. Grozin, *Sov. J. Part. Nucl.* **16**, 1 (1985); see also A.G. Grozin, *Z. Phys.* **C34**, 531 (1987).

[3] T. Hyer, *Phys. Rev.* **D48**, 147 (1993).

[4] S.J. Brodsky and G.R. Farrar, *Phys. Rev.* **D11**, 1309 (1975). See also P.V. Landshoff, *Phys. Rev.* **D10**, 1024 (1974), and A.H. Mueller, *Phys. Rept.* **73**, 237 (1981).

[5] Semiexclusive production of baryons is studied in A. Grozin, *Z. Phys.* **C34**, 531 (1987).

[6] D. Millers and J.F. Gunion, *Phys. Rev.* **D34**, 2657 (1986); A.S. Kronfeld and B. Nižić, *Phys. Rev.* **D44**, 3445 (1991).

[7] T. Hyer, *Phys. Rev.* **D47**, 3875 (1993).

[8] This naive definition ignores complications due to renormalization. However, the resulting formalism is still correct to leading twist; see Ref. [1].

[9] S. Gupta, *Phys. Rev.* **D24**, 1169 (1981). Baier and Grozin [2] have argued that Gupta's calculated amplitudes are incorrect; we do not use those results, only the proof of factorizability.

[10] Note that ϕ is not the azimuthal angle of the hadron; the latter does not enter into the amplitude.

[11] G.R. Farrar and F. Neri, *Phys. Lett.* **130B**, 109 (1983), *Phys. Lett.* **152B**, 443 (1984); see also M.L. Mangano and S.J. Parke, *Phys. Rept.* **200**, 301 (1991).

[12] E.D. Bloom and F.J. Gilman, *Phys. Rev. Lett.* **25**, 1140 (1970); *Phys. Rev.* **D4**, 2901 (1971).

[13] M.A. Shifman, A.I. Vaĭnshteĭn, and V.I. Zakharov, *Nucl. Phys.* **B147**, 385 (1979).

[14] V.L. Chernyak, A.R. Zhitnitsky, and I.R. Zhitnitsky, *Nucl. Phys.* **B204**, 477 (1982).

[15] A.R. Zhitnitskiĭ, I.R. Zhitnitskiĭ and V.L. Chernyak, *Sov. J. Nucl. Phys.* **38**, 775 (1983).

[16] V.L. Chernyak and A.R. Zhitnitsky, *Nucl. Phys.* **B246**, 52 (1984); I.D. King and C.T. Sachrajda, *Nucl. Phys.* **B297**, 785 (1987); V.L. Chernyak, A.A. Ogloblin, and I.R. Zhitnitskiĭ, *Sov. J. Nucl. Phys.* **48**, 536 (1988) [*Yad. Fiz.* **48**, 841 (1988)].

[17] V.L. Chernyak, A.A. Ogloblin, and I.R. Zhitnitskiĭ, *Z. Phys.* **C42**, 583 (1989); A.N. Kronfeld and B. Nižić, *Phys. Rev.* **D44**, 3445 (1991).

[18] The Gegenbauer polynomials C_i are customarily defined to be orthonormal over the interval $[-1,1]$ with measure $w(x) = (1-x^2)/4$ [1]. These are related to the functions P_i which we will use by $P_i(x) = \overline{2}C_i^{3/2}(x-\bar{x})$. We will continue to refer to the P_i as Gegenbauer polynomials.

[19] These may not appear to coincide with the polynomials listed in Ref. [3], because in this paper we explicitly show the overall factor $\overline{6}$, which Ref. [3] absorbed into the normalization factor.

[20] We are indebted to S. Brodsky for discussions of this point.

[21] S.J. Brodsky and G.P. Lepage, *Phys. Rev.* **D24**, 2848 (1981).

[22] J.D. Bjorken, *Phys. Rev.* **D47**, 101 (1993); J. Randa, *Phys. Rev.* **D21**, 1795 (1980).

[23] J.D. Bjorken, S.J. Brodsky, and H. Lu, *Phys. Lett.* **B286**, 153 (1993).

[24] Indeed, we may argue that such a 'background' event is itself intrinsically hard, so that any events containing such a gap are *ipso facto* semiexclusive. This is the viewpoint adopted by Baier and Grozin [2].

[25] This also allows for the possibility of the production of the meson in a Fock state with nonzero orbital angular momentum. As with helicity-flip terms, this will again contribute to the cross section at order $k_\perp^2/Q^2$.

[26] V.V. Sudakov, *Sov. Phys. – JETP* **3**, 65 (1956); A.H. Mueller, *Phys. Rept.* **73**, 237 (1981).

[27] There are indeed strong peaks in the inclusive cross section $\sigma_{\rm tot}(e^+e^- \to$ hadrons) above 2 GeV; however, they arise from heavy-quark resonances.

[28] J. Botts and G. Sterman, *Nucl. Phys.* **B325**, 62 (1989).

[29] A.R. Zhitnitskiĭ, I.R. Zhitnitskiĭ, and V.L. Chernyak, *Sov. J. Nucl. Phys.* **41**, 284 (1985) [*Yad. Fiz.* **41**, 445 (1985)].

[30] There is also a distribution $\phi_{3\rho}^A$, but it does not contribute to the process in which we are interested, in which the recoil q and $\bar{q}$ have opposite helicity.

[31] A.C. Mattingly and P.M. Stevenson, DE-FG05-92ER40717-7.

[32] S.J. Brodsky, G.P. Lepage, and P.B. Mackenzie, *Phys. Rev.* **D28**, 228 (1983).

[33] V.L. Chernyak and A.R. Zhitnitskiĭ, *Phys. Rept.* **112**, 173 (1984).

[34] Fermilab E665 Collaboration (M.R. Adams *et al.*), *Phys. Lett.* **287B**, 375 (1992).

[35] J. Botts, *Phys. Rev.* **D44**, 2768 (1992).

[36] See *e.g.* G. Farrar, E. Maina, and F. Neri, *Nucl. Phys.* **B259**, 702 (1985), *Nucl. Phys.* **B263**, 746 (1986).

[37] Reference [31] also displays an optimized third-order result for the coupling constant. However, we were unable to obtain numerical values or a parametric fit of this result, so we are compelled to use only the simpler form of Eq. (4.4).

[38] This conclusion actually holds only at leading logarithmic order; beyond that, corrections begin to depend on the details of the hard-scattering process from which the $q\bar{q}$ pair originates. However, such subleading corrections are outside the intended scope of this work.

[39] L.R. Surguladze and M.A. Samuel, *Phys. Rev. Lett.* **66**, 560 (1991); S.G. Gorishny, A.L. Kataev, and S.A. Larin, *Phys. Lett.* **259B**, 144 (1991).

[40] P.M. Stevenson, *Phys. Lett.* **100B**, 61 (1981).

[41] E. Berger, *Z. Phys.* **C4**, 289 (1980).

[42] EMC Collaboration (M. Arneodo *et al.*), *Nucl. Phys.* **B321**, 541 (1989).

[43] We note that tidal interactions proportional to $1/r^3$ are possible. However, they depend on the meson's having a nonzero average color dipole moment. Since we are attempting to determine the region in which multiple scattering is unimportant and the tree-level calculation of Eqs. (2.6)-(2.11) are trustworthy, we take at face value their implication that no color dipole moment is induced in the direct production process.

[44] G. Sterman and H. Li, *Nucl. Phys.* **B381**, 129 (1992); H. Li, ITP–SB–92–25.

[45] In fact, the cross section has the potential to exhibit a power-law dependence on $\Lambda_{\rm QCD}$, arising from the infrared behavior of $\alpha_{\rm eff}$. However, this threat never materializes. At moderate Q^2 ($Q \sim 10$ GeV), the suppression of $\alpha_{\rm eff}$

sets in before y becomes extremely small, while at large Q^2 (*e.g.* $Q = m_Z$) the jets inherit the parton momenta, and the small-y region will be excluded by experimental cuts. The insensitivity to $\Lambda_{\rm QCD}$ is demonstrated in our calculated cross sections, as described in Section 4.

[46] Intrinsically hard processes, such as direct production itself, are not expected to be well predicted by the Lund code. However, the hadronizing recoil system in which we are interested contains no such anomalies, so that our use of a Monte Carlo is justified.

[47] This idea was suggested to the author by J.D. Bjorken.

[48] Of course, this is equivalent to the requirement of a rapidity gap; the difference is one of notation, not of substance.

[49] The thrust actually lacks the transformation properties of a vector; nonetheless, we will persist in this notation.

[50] The behavior of the events from Eqs. (8.3) and (6.2) passing our cuts is similar, so that the value of $z_{\rm max}$ obtained in this way exhibits little dependence on the wavefunction.

[51] T. Hyer, SLAC-PUB-6383.

[52] M. A. Shifman, in *Aachen QCD Workshop 1992*, and references therein.

[53] M. A. Shifman and A. Voloshin, *Sov. J. Nucl. Phys.* **45**, 242 (1987) [*Yad. Fiz.* **45,** 463 (1987)]. The prediction $\langle x \rangle = 0.90$ GeV is consistent with the estimate $f_B = 90$ MeV also obtained in this reference.

[54] B. Jacobson, private communication.

[55] The integrands in A and $\bar{A}$ diverge at $x \to 0$ or 1, so that this metric does not yield a finite result unless the coefficients are constrained to yield a sum

which is finite at the endpoints (though it may fluctuate substantially near the limit).

[56] One might hope to compare the term $B = \int \phi(x)/x \, \mathrm{d}x$ from Eq. (B.1), which controls the process $\gamma_\uparrow \gamma_\uparrow \to K^- \bar{s}_- u_+$, with the corresponding $\bar{B} = \int \phi(x)/\bar{x} \, \mathrm{d}x$ which enters into the amplitude for $\gamma_\uparrow \gamma_\uparrow \to K^- \bar{s}_+ u_-$. However, in the region in which the assumption of duality is valid, it is *de facto* impossible to extract the spins of the hadronizing quarks; thus the only nonperturbative parameter which can be observed experimentally is the unpolarized sum $B^2 + \bar{B}^2$, which determines the absolute normalization.

[57] The derivation in Ref. [14] neglects the breaking of $SU(3)$ symmetry by the strange quark mass. No estimate of the symmetry-breaking quantities a_1 and a_3 is made.